SIMULATION OF TWO-DIMENSIONAL DIELECTRIC/METALLIC STRUCTURES WITH RESISTIVE SHEETS

Radiation Laboratory
The University of Michigan

Timothy J. Peters
John L. Volakis
Valdis V. Leipa

388967-4-T = RL-2559

SIMULATION OF TWO-DIMENSIONAL DIELECTRIC/METALLIC STRUCTURES WITH RESISTIVE SHEETS

TABLE OF CONTENTS

I. INTRODUCTION

The computation of the scattered field from two-dimensional inhomogeneous dielectric structures is traditionally accomplished via a direct numerical solution of the appropriate integral equations(IE). In the case of cylinders with arbitrary cross sections such solutions involve their discretization in terms of cells (cylinders of small cross section) of rectangular, trapezoidal or triangular cross section. For example, Richmond [1,2] used rectangular cells and introduced the volume equivalent electric currents assumed constant over each cell. These were then found via a matrix solution of the relevant integral equation for either polarization of incidence, and subsequently integrated to give the total scattered field. Schaubert et al [3] and Lang and Wilton [4] discretized the surface using triangular cells and a more suitable set of basic function before proceeding with a matrix solution of the IE.

When the two-dimensional structure of interest contains impenetrable surfaces, it is usually necessary to solve IEs involving both surface and line integrals. Certainly in the presence of only a perfectly conducting half plane, the use of line integrals may be eliminated via the introduction of an appropriate Green's function [5,6]. However, in general one cannot avoid the simultaneous presence of both types of integrals, a situation which may complicate the numerical solution of the integral equation, as well as the input data structure associated with the code.

An alternate numerical formulation is explored here for the modeling of two-dimensional dielectric structures which may contain any arbitrary configuration of perfectly conducting sections. It is based

on first subdividing the scatterer in thin layers of material, beginning from the outer surface. Each layer is then replaced with an equivalent resistive sheet [7,8] at the geometric center of the layer. This is illustrated in Fig. 1. A perfectly conducting section can be replaced by a resistive sheet of zero resistivity at the surface of the section (see Fig. 2). The electric currents supported by the resistive sheets are then evaluated via the application of the resistive boundary condition at each sheet.

It is the purpose of this report to demonstrate the validity of the aforementioned formulation. This will be accomplished by a comparison of its results with those obtained from the Volume I.E. [1,2], where applicable. As will be seen, the equivalent sheet formulation used to replace the dielectric layers comprising the structure is an adequate model for the evaluation of the scattered field from such structures. Furthermore, to treat materials having both dielectric and magnetic properties, the above concept is still applicable via the introduction of conductive sheets in addition to the resistive ones. This is not explored here and will be the subject of a subsequent investigation.

II. RESISTIVE SHEET BOUNDARY CONDITIONS

It has been established [7,9] that thin dielectric layers can be replaced by equivalent resistive sheets placed at the geometric center of the layer. Such resistive sheets carry an electric current

$$\bar{J} = \hat{n} \times [H]^{+}_{-} \tag{1}$$

where $[\ ]^{+}_{-}$ denotes the value of the quantity above and below the sheet. In addition, each sheet is characterized by the boundary condition

$$\hat{n} \times \bar{E} = R\hat{n} \times \bar{J} \tag{2}$$

where R is its assigned resistivity. Its value depends upon the material properties of the layer and is given by

$$R = \lim_{t \to o} \frac{-jZ_o}{k(\varepsilon_r - 1)t} \tag{3}$$

where t is the thickness of the layer, ε_r is the relative dielectric constant and Z_o is the free space impedance. Equation (3) is suitable for

lossy materials. However, in the case of lossless or only slightly lossy materials, we found that a more accurate choice for R is ($e^{j\omega t}$)

$$R = -\frac{1}{2}\left[\frac{e^{-jkt}}{r} + 1\right] \tag{4}$$

with

$$r = \frac{\Gamma\left(1-P_d^2\right)}{1-\left(\Gamma P_d\right)^2} \quad , \tag{5}$$

where

$$\Gamma = \frac{1-\sqrt{\varepsilon_r}}{1+\sqrt{\varepsilon_r}} \tag{6}$$

is the plane wave reflection coefficient of a dielectric half space and

$$P_d = e^{-jkt\sqrt{\varepsilon_r}} \quad . \tag{7}$$

Equation (4) was derived by requiring that the reflected fields from the dielectric layer or the resistive sheet, are equal (see Appendix A). Equations (3) and (4) overlap for a loss tangent of approximately 0.2, and for loss tangents above this (3) should be used.

When considering H_z - incidence, it has been suggested [9] that for a thin layer (1)-(3) should be complemented by the additional boundary condition

$$-\hat{\ell}\cdot[\overline{E}^{+}-\overline{E}^{-}] = \frac{t}{2}\left(1-\frac{1}{\varepsilon_r}\right)\frac{\partial}{\partial\ell}[\hat{n}\cdot(\overline{E}^{+}+\overline{E}^{-})] \tag{8}$$

where $\frac{\partial}{\partial\ell}$ denotes differentiation with respect to the direction tangent to the sheet. Equ. (8) demands continuity of the normal derivative of H_z implying the existance of a magnetic current, $\overline{M}$, given by

$$\hat{z}\cdot\overline{M} = \frac{t}{2}\left(1-\frac{1}{\varepsilon_r}\right)\frac{\partial}{\partial\ell}[\hat{n}\cdot(E^{+}+\overline{E}^{-})] \tag{9}$$

where $\overline{E}^{\pm}$ denotes the electric field above or below the dielectric layer. Clearly, $\overline{M}$ is proportional to the second derivative of H_z.

The magnetic currents in (9) are certainly much smaller than the electric currents in (2) and will therefore be neglected in the present study. However, it will be shown later that they are necessary in the case of materials with small loss.

III. E_z-INCIDENCE INTEGRAL EQUATION

The scattered field due to the induced current, J_z, on the sheets is given by

$$E_z^s = -\frac{kZ_o}{4}\int_{\ell'} J_z(\ell')H_o^{(2)}(k|\bar{\rho}-\bar{\rho}'|)d\ell', \tag{10}$$

where $H_o^{(2)}$ denotes the Hankel function,

$$\bar{\rho} = x\hat{x} + y\hat{y},$$

$$\bar{\rho}' = x'\hat{x} + y'\hat{y}, \tag{11}$$

$$x = f(\ell),\ y = g(\ell),$$

with (x,y) & (x',y') being the observation and integration points, respectively. Note that 11(c) are the parametric equations for the sheets and the integration is, of course, performed over all resistive sheets. Application of (2) gives [10,11].

$$R(\ell)J_z(\ell)+\frac{kZ_o}{4}\int_{\ell'} J_z(\ell')H_o^{(2)}(k|\bar{\rho}-\rho'|)d\ell' = E_z^i(\ell) \tag{12}$$

where $E_z^i(x,y)$ is the incident field. Equation (12) can now be solved numerically to evaluate the unknown currents. The details of the solution are given in Appendices C and D. Specifically, the current is first expanded using pulse basis function as

$$J_z(\ell) = \sum_{m=1}^{M} J_m \; P_{\frac{\delta}{2}}(\ell-\ell_m) \tag{13}$$

with

$$P_{\frac{\delta}{2}}(\ell) = \begin{cases} 1 & -\frac{\delta}{2} < \ell < \frac{\delta}{2} \\ 0 & \text{otherwise.} \end{cases} \tag{14}$$

It is then substituted in (12) which is enforced at M points to generate an equal number of equations for computing the M unknowns, J_m. The point matching technique is employed to obtain a set of equations which can be written in the usual form

$$[J]\,[Z] = [V] \tag{15}$$

where [Z] is a square matrix, referred to as the impedance matrix. [V] is the excitation column vector and [J] is the column of the unknown current elements.

Once the current is found, the radar cross section (RCS) at an angle ϕ is computed using the equation

$$\sigma_E = \lim_{\rho\to\infty} 2\pi\rho \left|\frac{E_z^s}{E_z^i}\right|^2 = \frac{k}{4}(\delta Z_o)^2 \left| \sum_{m=1}^{M} J_m e^{jk[f(\ell_m)\cos\phi + g(\ell_m)\sin\phi]} \right|^2$$

The E_z-case integral equation solution is implemented in the computer code REST–E (see Appendix C).

IV. H_z-INCIDENCE INTEGRAL EQUATION

For the H_z-incidence, the scattered field is represented by

$$E^s = -\frac{Z_o}{4}\left(\frac{\partial}{\partial n}\hat{\ell} - \frac{\partial}{\partial \ell}\hat{n}\right)\int_{\ell'}(\hat{n}'\cdot\hat{r})\, J_{\ell'}(\ell')\, H^{(2)}\, k|\bar{\rho}-\bar{\rho}'|d\ell', \tag{17}$$

where

$$\hat{r} = \frac{\bar{\rho}-\bar{\rho}'}{|\bar{\rho}-\bar{\rho}'|}, \tag{18}$$

is, as usual, tangent to the sheets (also normal to $\hat{z}$) and $J_\ell(\ell)$ is the induced current on the sheets.

Application of the boundary condition (2) yields the integral equation [10,11]

$$\frac{4R(\ell)}{Z_o} J_\ell(\ell) + \frac{\partial}{\partial n}\int_{\ell'}(\hat{n}'\cdot\hat{r})J_{\ell'}(\ell')H_1^{(2)}(k|\bar{\rho}-\bar{\rho}'|)d\ell' = \frac{4}{Z_o}E^i_\ell(\ell) \tag{19}$$

This can again be solved numerically for the evaluation of the currents $J_\ell(\ell)$ in a similar manner to that described for the E_z - incidence. The details of the numerical solution are given in Appendices C and E. However, we do note that the evaluation of the resulting self cell integrals requires more careful attention.

Once the sheet currents are found, the radar cross section at an angle ϕ is given by

$$\sigma_H = \lim_{\rho\to\infty} 2\pi\rho\left|\frac{H_z^s}{H_z^i}\right|^2 = \frac{k}{4}(\delta \sin\phi)^2\left|\sum_{m=1}^{M} J_m e^{jk\left[f(\ell_m)\cos\phi + g(\ell_m)\sin\phi\right]}\right|^2 \tag{20}$$

The H_z-incidence solution of the integral equation is implemented in the computer code REST H (see Appendix C).

V. SIMULATION OF A THICK DIELECTRIC SLAB WITH RESISTIVE SHEETS

The thick rectangular slab was used as a test case for exploring the capability of multiple sheets to simulate thick material. Based on earlier discussions, the slab was layered as shown in Figure 3 and each dielectric layer was then replaced with an equivalent resistive sheet. Both E_z and H_z incidences were examined.

The results of the REST codes were compared with those obtained via the numerical solution of the Volume I.E. described in Richmond [1,2]. Comparison of results was not restricted to data published in [1,2] because the simulation of the corresponding geometries via resistive sheets would be a rather trivial case. Therefore, since the codes based on the Volume I.E.'s were not available from the original author, they were generated anew. The details of the study relating to the E_z incidence are included in Appendices A and B. Below we only summarize the results of this study.

In the case of E_z-incidence, it was confirmed that the resistive sheet formulation is identical to the volume integral equation, where applicable. This was established not only via the comparison of numerical results but also analytically.

In the case of H_z incidence, we found that the resistive sheet alone is not adequate for replacing the dielectric layer. This is especially true for low loss dielectrics. However, it was established that the sheet methodology is still a valid formulation. Particularly, in addition to the resistive sheet, a magnetic current sheet, given by (9), is also necessary to accurately model the presence of a dielectric

layer with the H_z-incidence. Based on this conclusion, a pair of coupled line integral equations were derived to replace the more cumbersome surface integral equations [2]. The numerical implementation of the coupled line integral equations is currently in progress.

REFERENCES

1. J.H. Richmond, "Scattering by a Dielectric Cylinder of Arbitrary Cross Section Shape," IEEE Trans on Antennas and Propagation, Vol. AP-13, pp. 334-341, May 1965

2. J.H. Richmond, "TE-Wave Scattering by a Dielectric Cylinder of Arbitrary Cross Section Shape," IEEE Trans. on Antennas and Propagation, Vol. AP-14, pp. 460-464, July 1966.

3. D.H. Schaubert, D.R. Wilton, and A.W. Glisson, "A Tetrahedral Modeling Method for Electromagnetic Scattering by Arbitrarily Shaped Inhomogeneous Dielectric Bodies," IEEE Trans. on Antennas and Propagation, Vol. AP-32, pp 77-85, Jan. 1985

4. D.K. Langan and D.R. Wilton, "Numerical Solution of TE Scattering by Inhomogeneous Two-Dimensional Composite Dielectric/Metallic Bodies of Arbitrary Cross Section", presented at the 1986 National Radio Science Meeting, Philadelphia, PA, 1986.

5. E.H. Newman, "TM Scattering by a Dielectric Cylinder in the Presence of a Half Plane," IEEE Trans. on Angennas and Propagation, Vol. AP-33, pp. 773-782, July 1985.

6. E.H. Newman, "TM and TE Scattering by a Dielectric/Ferrite Cylinder in the Presence of a Half-Plane," IEEE Trans. on Antennas and Propagation, Vol. AP-34, pp. 804-813, June 1986

7. R.F. Harrington and J.R. Mautz, "An Impedance Sheet Approximation of the Dielectric Shells", IEEE Trans, on Antennas and Propagation, Vol. AP-23, pp. 531-534, 1975.

8. T.B.A. Senior, "Combined Resistive and Conductive Sheets", IEEE Trans on Antennas and Propagation, Vol. AP-33, pp. 577-579, 1985.

9. F.G. Leppington, "Travelling Waves in a Dielectric Slab With An Abrupt Change in Thickness," Proc. Roy. Soc. London, 386(A), pp. 443-460, 1983.

10. M.I. Herman and J.L. Volakis, "High Frequency Scattering by a Resistive Strip", The University of Michigan Radiation Laboratory Report 388967-3-T, 1986.

11. V.V. Liepa, E.F. Knott and T.B.A. Senior, "Scattering From Two-Dimensional Bodies With Absorber Sheets," The University of Michigan Radiation Laboratory Report 011764-2-T, 1974.

12. T.B.A. Senior and V.V. Liepa, "Non-Specular RAM," The University of Michigan Radiation Laboratory Report 014518-1-F, April 1977.

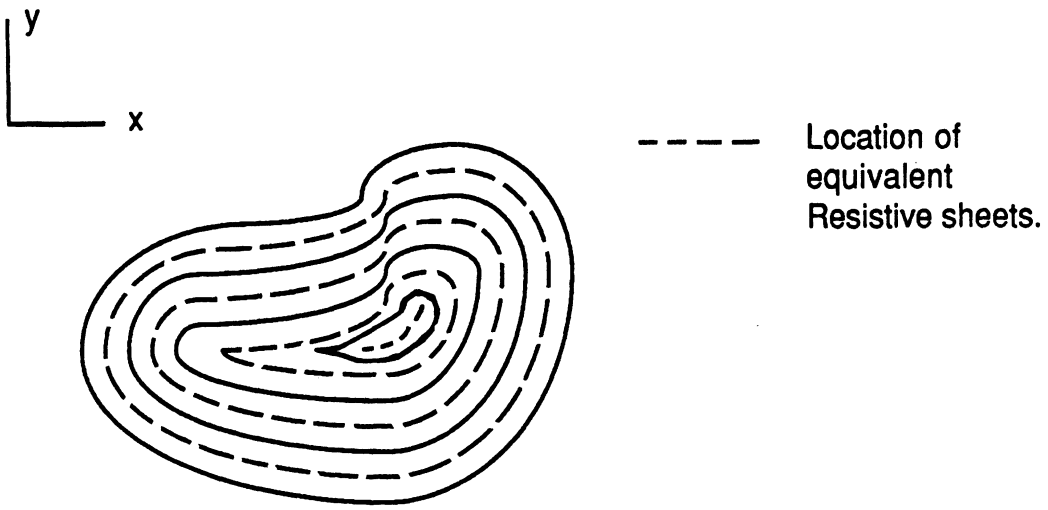

Fig. 1. Illustration of the layering of dielectric cylinder.

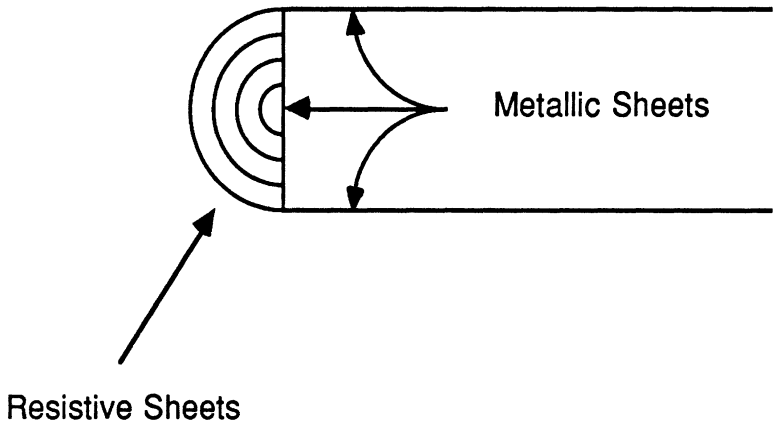

Fig. 2. Junctions of Metallic/Resistive Sheets.

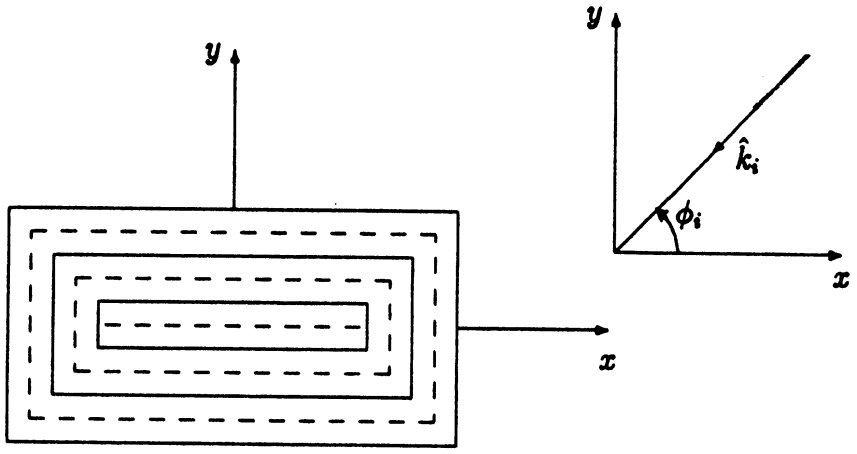

Fig. 3. Simulation of a dielectric cylinder with resistive sheets at the geometric center of each layer.

Appendices

All appendices should be considered as self contained units. Equation and figure numbers are reset at the beginning of each appendix. Also, all references quoted in an appendix may be found at the end of that appendix.

Appendix A - Thick Dielectric Slab REST-E vs Volume I.E.

I. Simulation of Dielectric Slab

Dielectric cylinders may be effectively modeled by segmenting the cylinder into layers and placing resistive strips at the geometric mean of each layer.

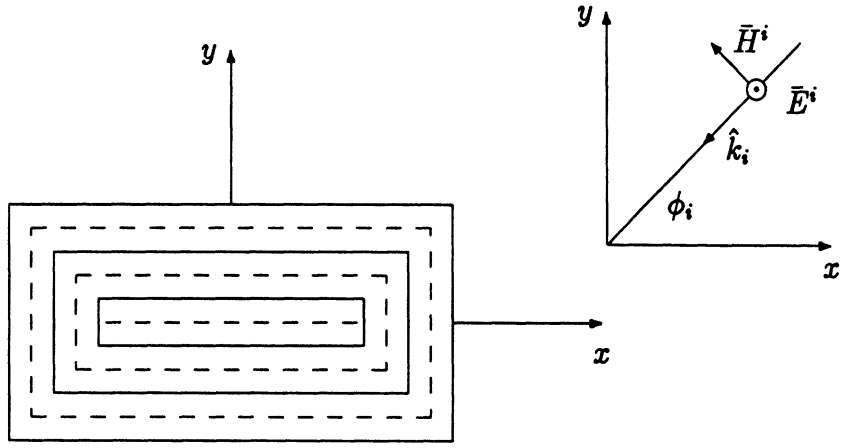

Fig. 1. Dielectric cylinder with strips placed at the geometric center of each layer

Both models involve formulation and solution of an inhomogeneous Fredholm equation of the second kind. The volume integral equation is [1]

$$\frac{4}{k_0 Z_0} E_z(x,y) + \int\int_{S'} J_z(x',y') H_0^{(2)}(k_0\rho) dx'dy' = \frac{4}{k_0 Z_0} E_z^i(x,y) \tag{1}$$

where

$$J_z(x',y') = j\frac{k_0}{Z_0}\left(\epsilon_r(x',y') - 1 - j\frac{\sigma(x',y')}{\omega\epsilon_0}\right) E_z(x',y') \tag{2}$$

and $\rho = \sqrt{(x-x')^2 + (y-y')^2}$. The analogous resistive strip equation is [2]

$$\frac{4}{k_0}\eta(x,y) K_z(x,y) + \int_{l'} K_z(x',y') H_0^{(2)}(k_0\rho) dl' = \frac{4}{k_0 Z_0} E_z^i(x,y) \tag{3}$$

where

$$\eta(x,y) = \frac{-j}{\left(\epsilon_r(x,y) - 1 - j\frac{\sigma(x,y)}{\omega\epsilon_0}\right) k_0 d} \tag{4}$$

and ρ is the same as (1). Numerical computations have shown that placing the strip at the geometric mean of the layer yields the least error. Computational efficiency may be improved by calculating the strip resistance using two different models contingent on the loss tangent. The resistance for low loss dielectrics is calculated by matching the physical optics reflection and transmission coefficients with the corresponding coefficients for a resistive strip. For high loss dielectrics the surface resistance may be derived directly from Maxwells equations by considering equivalent polarization and conduction currents. The test results indicate that for a loss tangent of approximately 0.25 both models are valid and yield the same results. Also, a slab layer width of $0.1\lambda_s$, where λ_s is the wavelength in the medium, was found to yield excellent agreement between the two models. However, this constraint may be relaxed if the material has a

high loss tangent.

II. Derivation of Z_s Based on Physical Optics

For low loss dielectrics the convergence of the solution, in terms of the number of cells required, may be improved by considering the physical optics model based on Fig. 2 and Fig. 3.

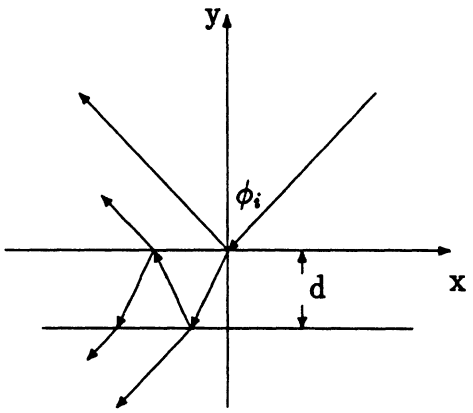

Fig. 2. Plane wave incident on dielectric slab

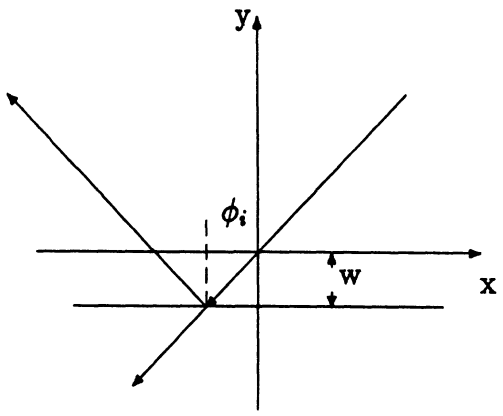

Fig. 3. Plane wave incident on resistive strip

The reflection and transmission coefficients for the infinite dielectric slab shown in Fig. 2 may be obtained by summing the contributions due to all rays [3]. The standard Fresnel reflection coefficient for $d = \infty$ is

$$\Gamma_\perp = \frac{cos(\phi_i) - \sqrt{\epsilon_r - j\frac{\sigma}{\omega\epsilon_0} - sin^2(\phi_i)}}{cos(\phi_i) + \sqrt{\epsilon_r - j\frac{\sigma}{\omega\epsilon_0} - sin^2(\phi_i)}} \tag{5}$$

where the relation $R = 1 - T$ can be used to calculate the transmission coefficient.

The total reflection and transmission coefficients for the slab are given by

$$R_\perp = \frac{\Gamma_\perp(1-P_d^2P_a)}{1-\Gamma_\perp^2P_d^2P_a} \tag{6}$$

$$T_\perp = \frac{\Gamma_\perp(1-P_d^2P_t)}{1-\Gamma_\perp^2P_d^2P_a} \tag{7}$$

where

$$P_d = e^{-jk_0d\frac{\epsilon_r-j\frac{\sigma}{\omega\epsilon_0}}{\sqrt{\epsilon_r-j\frac{\sigma}{\omega\epsilon_0}-sin^2(\phi_i)}}} \tag{8}$$

$$P_a = e^{j2k_0d\frac{sin^2(\phi_i)}{\sqrt{\epsilon_r-j\frac{\sigma}{\omega\epsilon_0}-sin^2(\phi_i)}}} \tag{9}$$

$$P_t = e^{jk_0d\left(cos(\phi_i)+\frac{sin^2(\phi_i)}{\sqrt{\epsilon_r-j\frac{\sigma}{\omega\epsilon_0}-sin^2(\phi_i)}}\right)}. \tag{10}$$

The reflection and transmission coeffecients for the resistive strip shown in Fig. 3 may be easily derived and are

$$R_\perp = -\frac{Z_0e^{-j2k_0Wcos(\phi_i)}}{Z_0+2Z_s^\perp cos(\phi_i)} \tag{11}$$

$$T_\perp = \frac{2Z_scos(\phi_i)}{Z_0+2Z_s^\perp cos(\phi_i)} \tag{12}$$

where Z_s is such that the coefficients (6)-(7) match (11)-(12) at $\phi_i = 0$. Thus, solving (11) the surface resistance is

$$Z_s^\perp = -\frac{Z_0}{2R_\perp}\left[R_\perp(\phi_i=0)+e^{-jk_0d}\right]. \tag{13}$$

III. Derivation of Z_s Based on Polarization and Conduction Currents

Consider the decomposition of the Maxwell equation

$$\begin{aligned}\nabla\times\bar{H} &= \bar{J}+j\omega\bar{D}\\ &= \sigma\bar{E}+j\omega\epsilon_0\bar{E}+j\omega\bar{P}\\ &= \sigma\bar{E}+j\omega\epsilon_0\bar{E}+j\omega\epsilon_0(\epsilon_r-1)\bar{E}\\ &= j\omega\epsilon_0\left(\epsilon_r-1-j\frac{\sigma}{\omega\epsilon_0}\right)\bar{E}+j\omega\epsilon_0\bar{E}.\end{aligned} \tag{14}$$

Assume a scattered field due to an equivalent current

$$\bar{J}_{eq} = j\omega\epsilon_0 \left(\epsilon_r - 1 - j\frac{\sigma}{\omega\epsilon_0}\right) \bar{E}. \tag{15}$$

This represents current flow due to polarization and conduction [4].

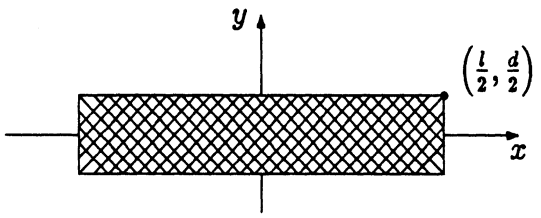

Fig. 4. Dielectric slab.

Given the geometry of Fig. 4 for $d \ll \lambda_s \ll l$, in the limit as $d \to 0$ (15) may be written as

$$\begin{aligned} E_z(x, y=0) &= \frac{1}{j\omega\epsilon_0 \left(\epsilon_r - 1 - j\frac{\sigma}{\omega\epsilon_0}\right)} \lim_{d\to 0} J_z(x, y=0) \\ &= \frac{-jZ_0}{\left(\epsilon_r - 1 - j\frac{\sigma}{\omega\epsilon_0}\right) k_0 d} K_z \\ &= Z_s K_z. \end{aligned} \tag{16}$$

Where the surface resistance Z_s may now be defined as

$$Z_s = \frac{-jZ_0}{(\epsilon_r - 1 - j\frac{\sigma}{\omega\epsilon_0}) k_0 d}. \tag{17}$$

IV. Test Results

A number of backscattering patterns were generated by the strip model for a rectangular slab and to verify their validity they were compared with results obtained by the volume integral method [1]. The validity of [1] has been established provided convergence with respect to the sampling rate is attained. All

calculations were performed for a homogeneous (not a restriction) dielectric slab of length $l = 2\lambda_0$, width d and permitivity $\epsilon = \epsilon_0 \left(\epsilon_r - j\frac{\sigma}{\omega\epsilon_0}\right)$. The individual cases are listed in Table 1. Each of the figures contains a backscattering pattern at $\phi_i = 0°$ (edge on incidence) to $\phi_i = 90°$ (normal incidence). The figure captions describe the input data as well as the size and condition number κ of the computed N $\times$ N matrix. The results show excellent agreement between the two formulations.

Test Cases			
Figure	d	$\frac{\epsilon}{\epsilon_0}$	loss tangent
5	$0.01\lambda_0 = 0.01\lambda_s$	1.0-j9999.0	9999.000
6	$0.1\lambda_0 = 0.14\lambda_s$	2.0-j10.0	5.000
7	$0.1\lambda_0 = 0.14\lambda_s$	2.0-j2.0	1.000
8	$0.1\lambda_0 = 0.14\lambda_s$	2.0-j1.6	0.800
9	$0.1\lambda_0 = 0.14\lambda_s$	2.0-j1.2	0.600
10	$0.1\lambda_0 = 0.14\lambda_s$	2.0-j0.8	0.400
11	$0.1\lambda_0 = 0.14\lambda_s$	2.0-j0.4	0.200
12	$0.1\lambda_0 = 0.14\lambda_s$	2.0-j0.0	0.000
13	$0.5\lambda_0 = 1.00\lambda_s$	4.0-j0.5	0.125
14	$0.5\lambda_0 = 1.25\lambda_s$	6.0-j1.0	0.167
15	$0.5\lambda_0 = 1.58\lambda_s$	8.0-j2.0	0.250
16	$0.5\lambda_0 = 1.58\lambda_s$	10.0-j3.0	0.300

Table 1.

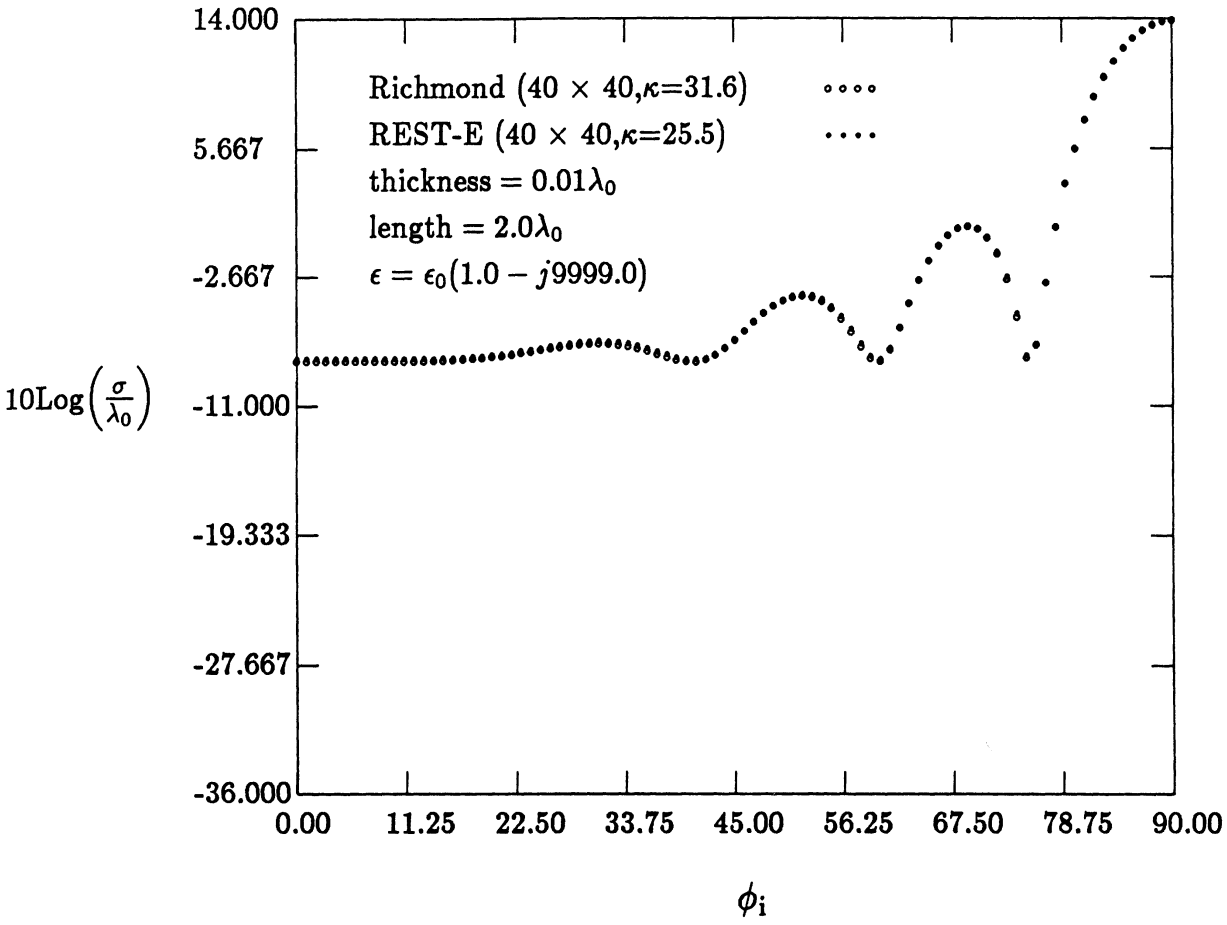

Fig. 5.

The volumetric model appears to be able to accurately simulate a perfectly conducting strip. Note that the physical optics solution for a $d = 2\lambda_0$ perfectly conducting strip is given as

$$\begin{aligned} \sigma_{db} &= 10\text{Log}\left(2\pi\frac{d^2}{\lambda_0^2}\right) \\ &= 14.0023. \end{aligned} \tag{18}$$

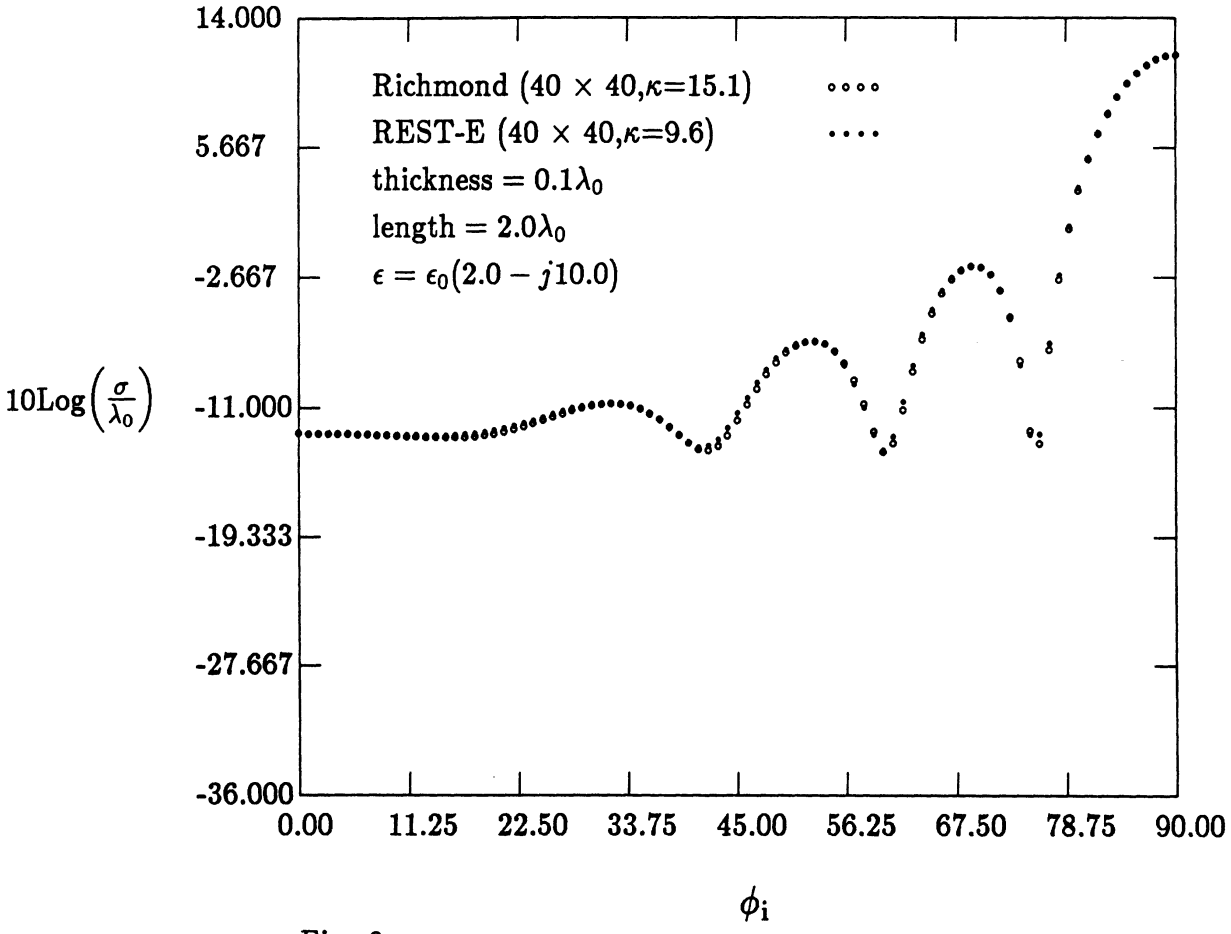
14.000
5.667
-2.667
-11.000
-19.333
-27.667
-36.000
0.00
11.25
22.50
33.75
45.00
56.25
67.50
78.75
90.00
Richmond (40 × 40,κ=15.1)
REST-E (40 × 40,κ=9.6)
thickness = 0.1λ0
length = 2.0λ0
ε = ε0(2.0 − j10.0)
10Log(σ/λ0)
φi

Fig. 6.

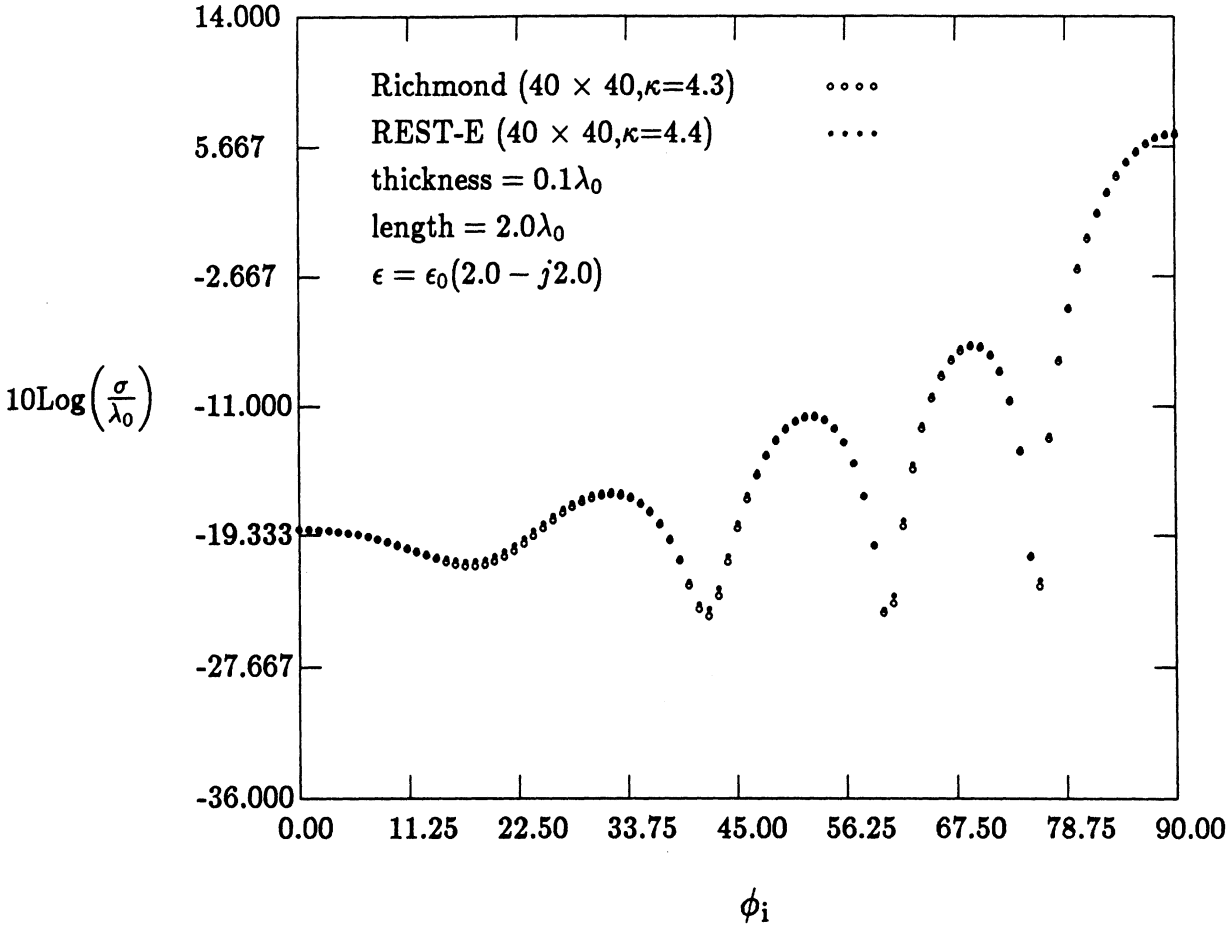
14.000
5.667
-2.667
-11.000
-19.333
-27.667
-36.000
0.00
11.25
22.50
33.75
45.00
56.25
67.50
78.75
90.00
Richmond (40 × 40,κ=4.3)
REST-E (40 × 40,κ=4.4)
thickness = 0.1λ0
length = 2.0λ0
ε = ε0(2.0 − j2.0)
10Log(σ/λ0)
φi

Fig. 7.

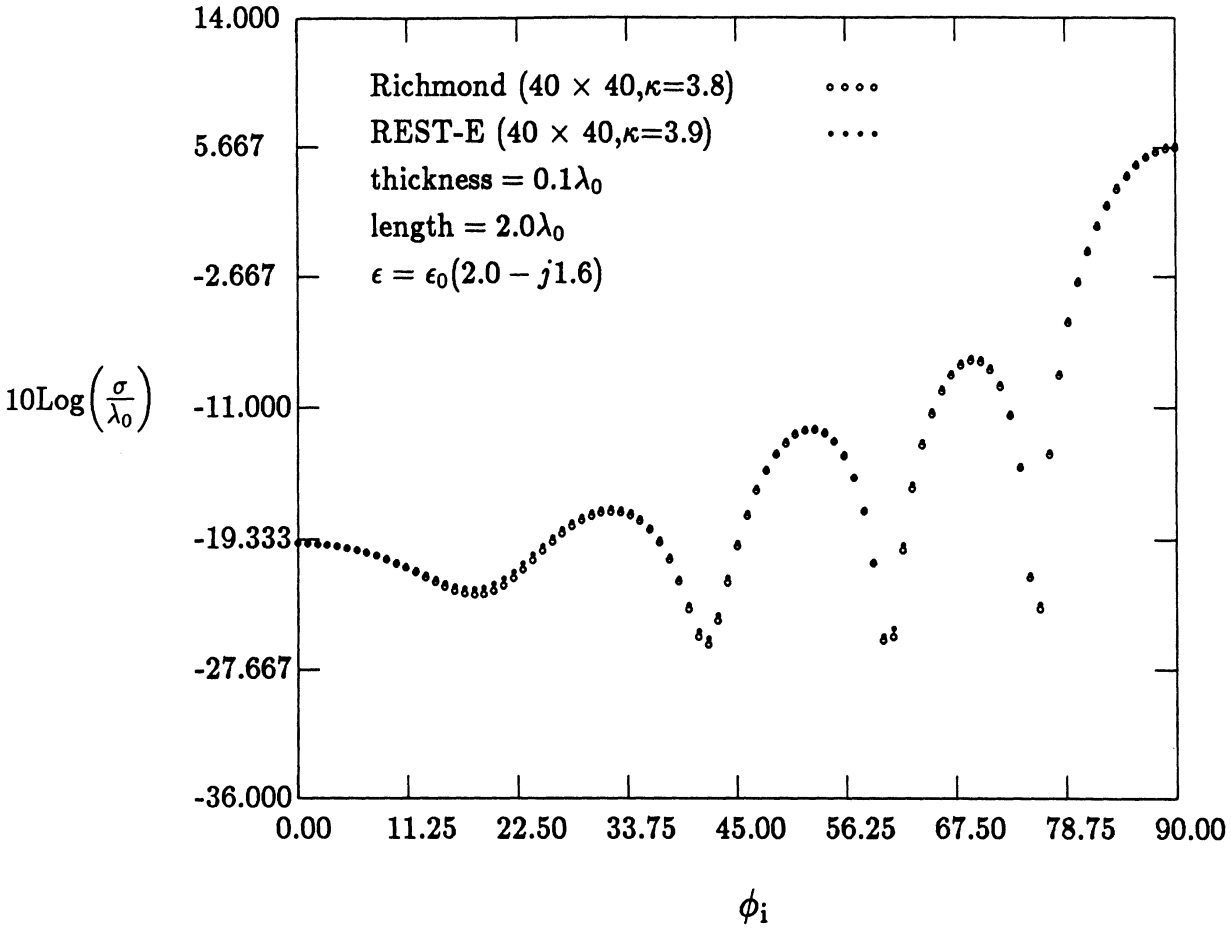
14.000
5.667
-2.667
-11.000
-19.333
-27.667
-36.000
0.00
11.25
22.50
33.75
45.00
56.25
67.50
78.75
90.00
Richmond (40 × 40,κ=3.8)
REST-E (40 × 40,κ=3.9)
thickness = 0.1λ0
length = 2.0λ0
ϵ = ϵ0(2.0 − j1.6)
10Log(σ/λ0)
φi

Fig. 8.

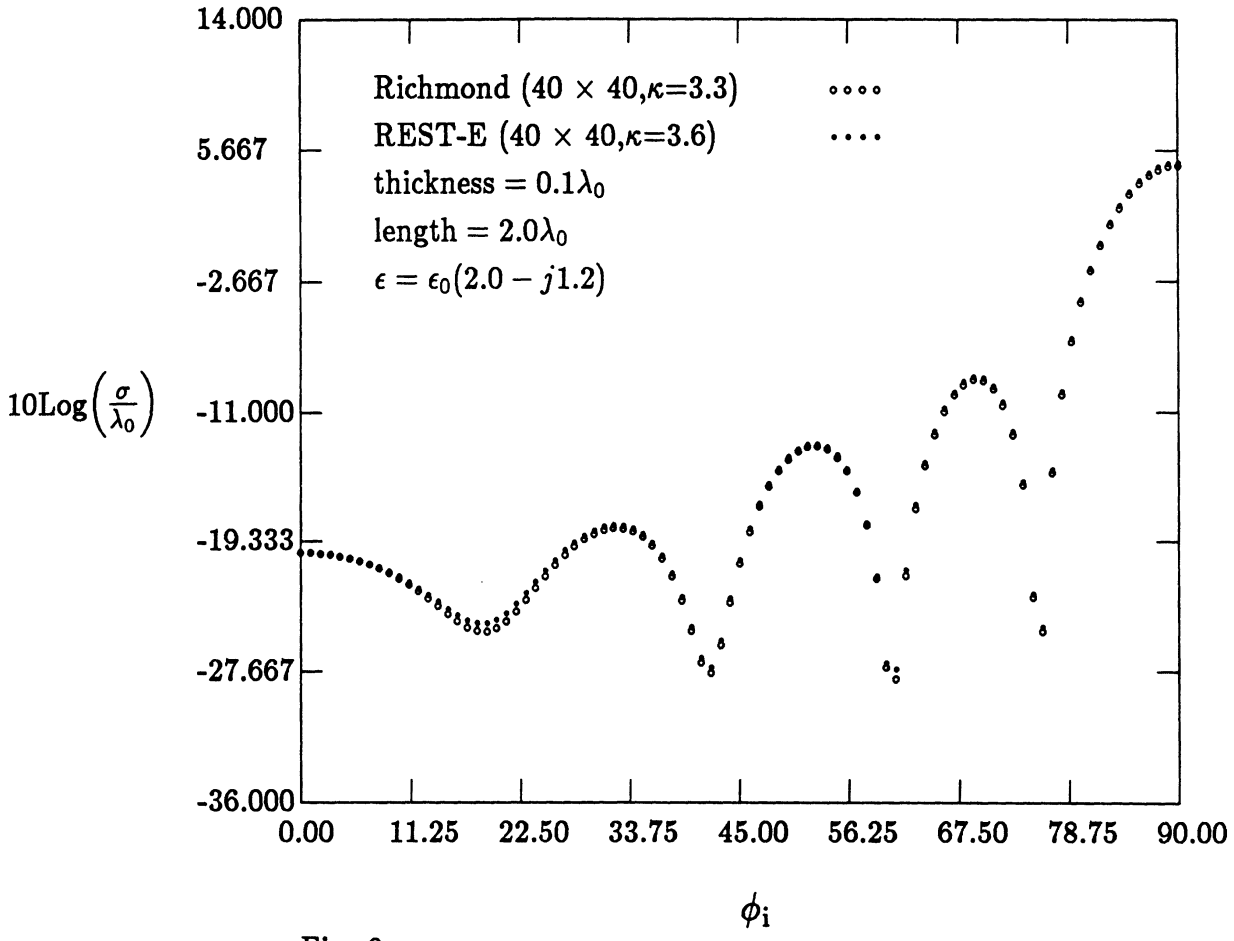
14.000
5.667
-2.667
-11.000
-19.333
-27.667
-36.000
0.00
11.25
22.50
33.75
45.00
56.25
67.50
78.75
90.00
Richmond (40 × 40,κ=3.3)
REST-E (40 × 40,κ=3.6)
thickness = 0.1λ0
length = 2.0λ0
ε = ε0(2.0 − j1.2)
10Log(σ/λ0)
φi

Fig. 9.

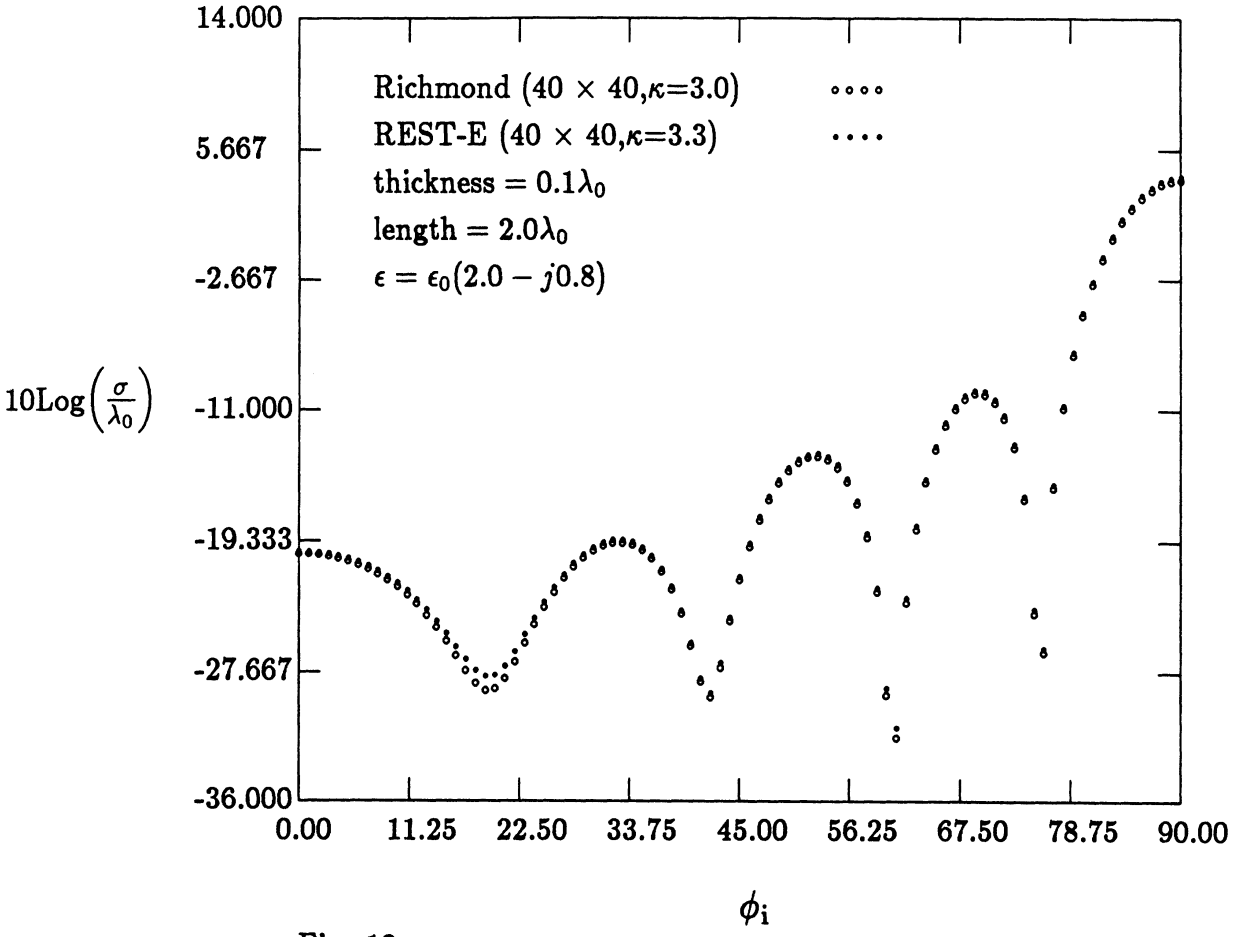
14.000
5.667
-2.667
-11.000
-19.333
-27.667
-36.000
0.00
11.25
22.50
33.75
45.00
56.25
67.50
78.75
90.00
Richmond (40 × 40,κ=3.0)
REST-E (40 × 40,κ=3.3)
thickness = 0.1λ0
length = 2.0λ0
ε = ε0(2.0 − j0.8)
10Log(σ/λ0)
φi

Fig. 10.

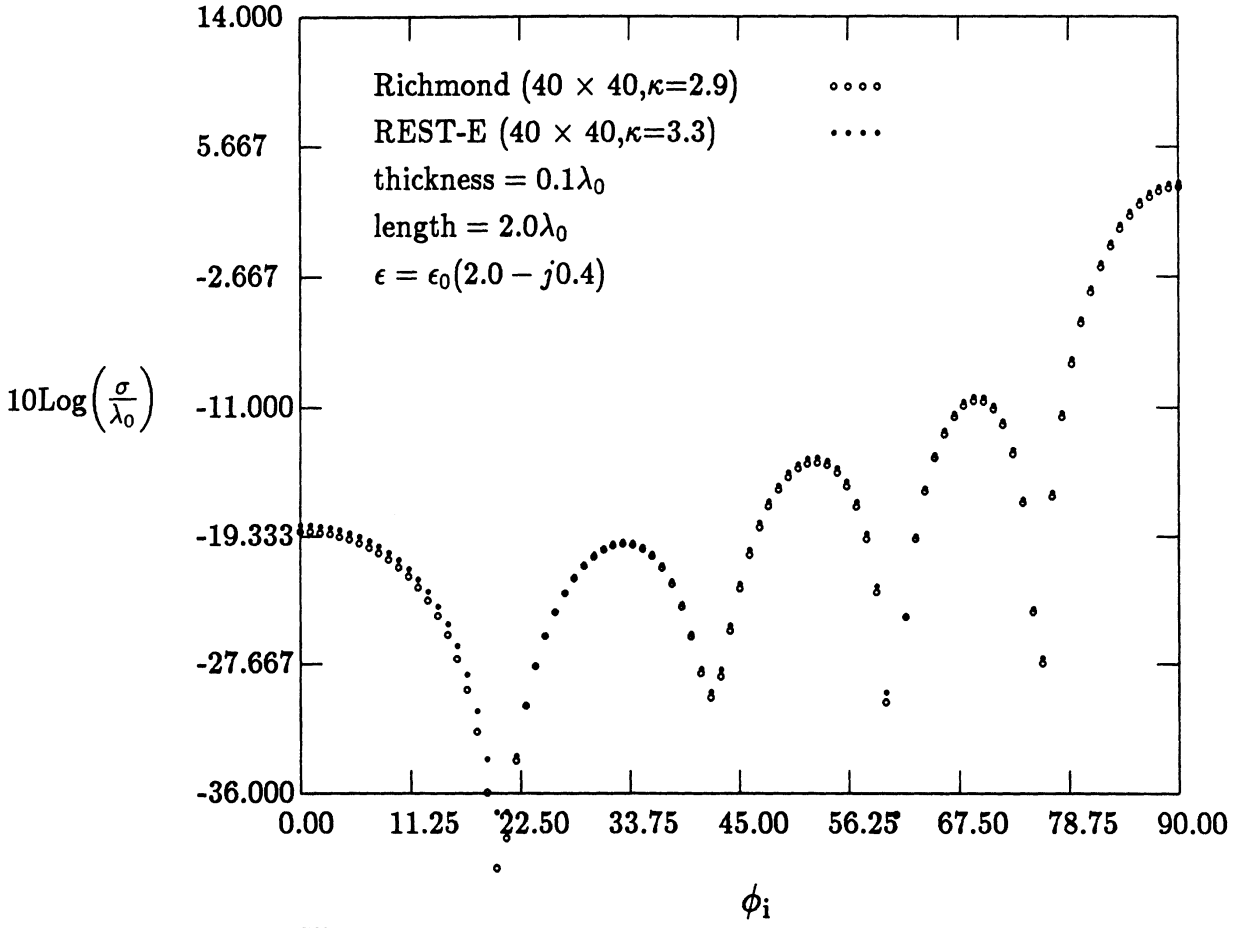
14.000
5.667
-2.667
-11.000
-19.333
-27.667
-36.000
Richmond (40 × 40,κ=2.9)
REST-E (40 × 40,κ=3.3)
thickness = 0.1λ0
length = 2.0λ0
ε = ε0(2.0 − j0.4)
10Log(σ/λ0)
0.00
11.25
22.50
33.75
45.00
56.25
67.50
78.75
90.00
φi

Fig. 11.

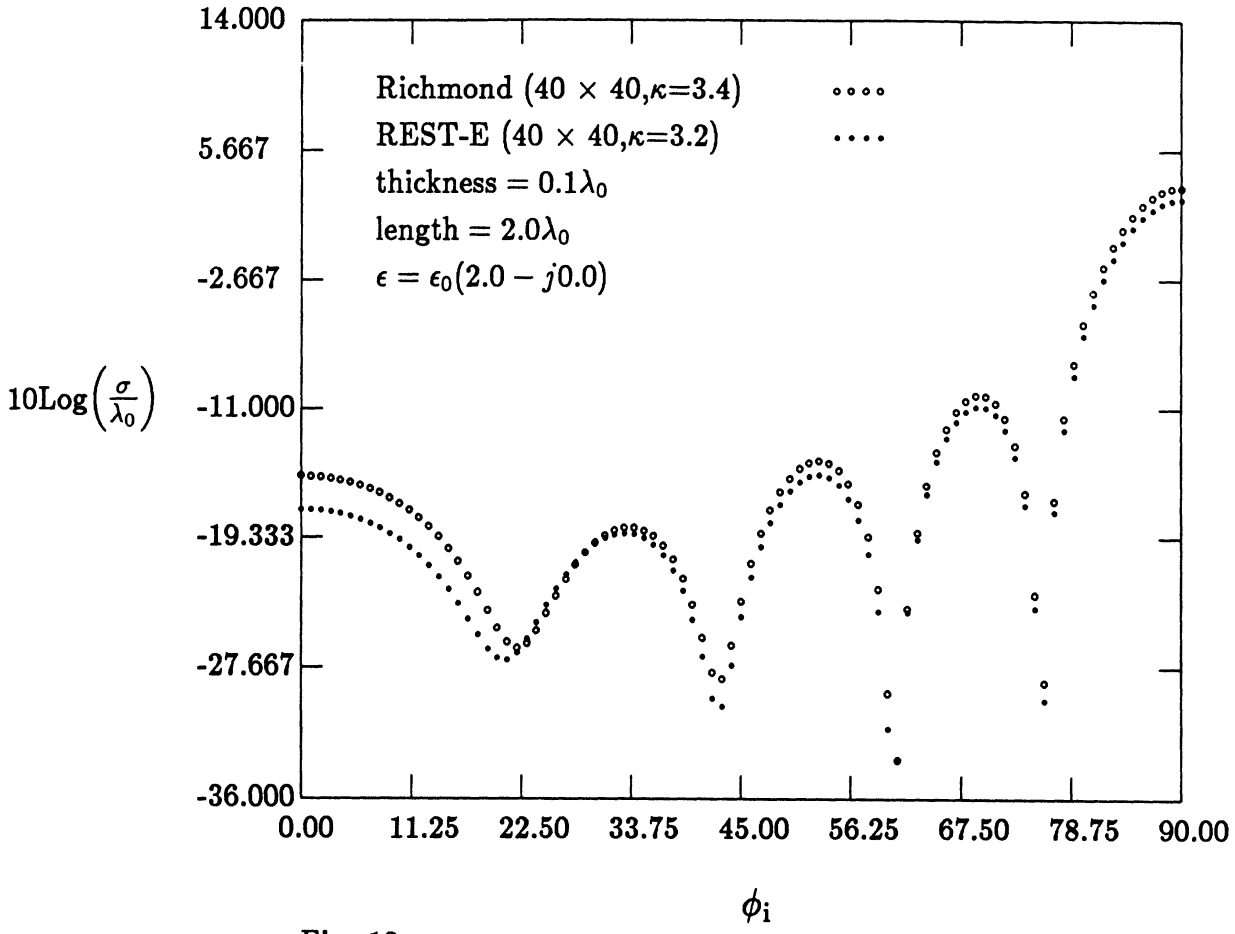
14.000
5.667
-2.667
-11.000
-19.333
-27.667
-36.000
0.00
11.25
22.50
33.75
45.00
56.25
67.50
78.75
90.00
Richmond (40 × 40,κ=3.4)
REST-E (40 × 40,κ=3.2)
thickness = 0.1λ0
length = 2.0λ0
ε = ε0(2.0 − j0.0)
10Log(σ/λ0)
φi

Fig. 12.

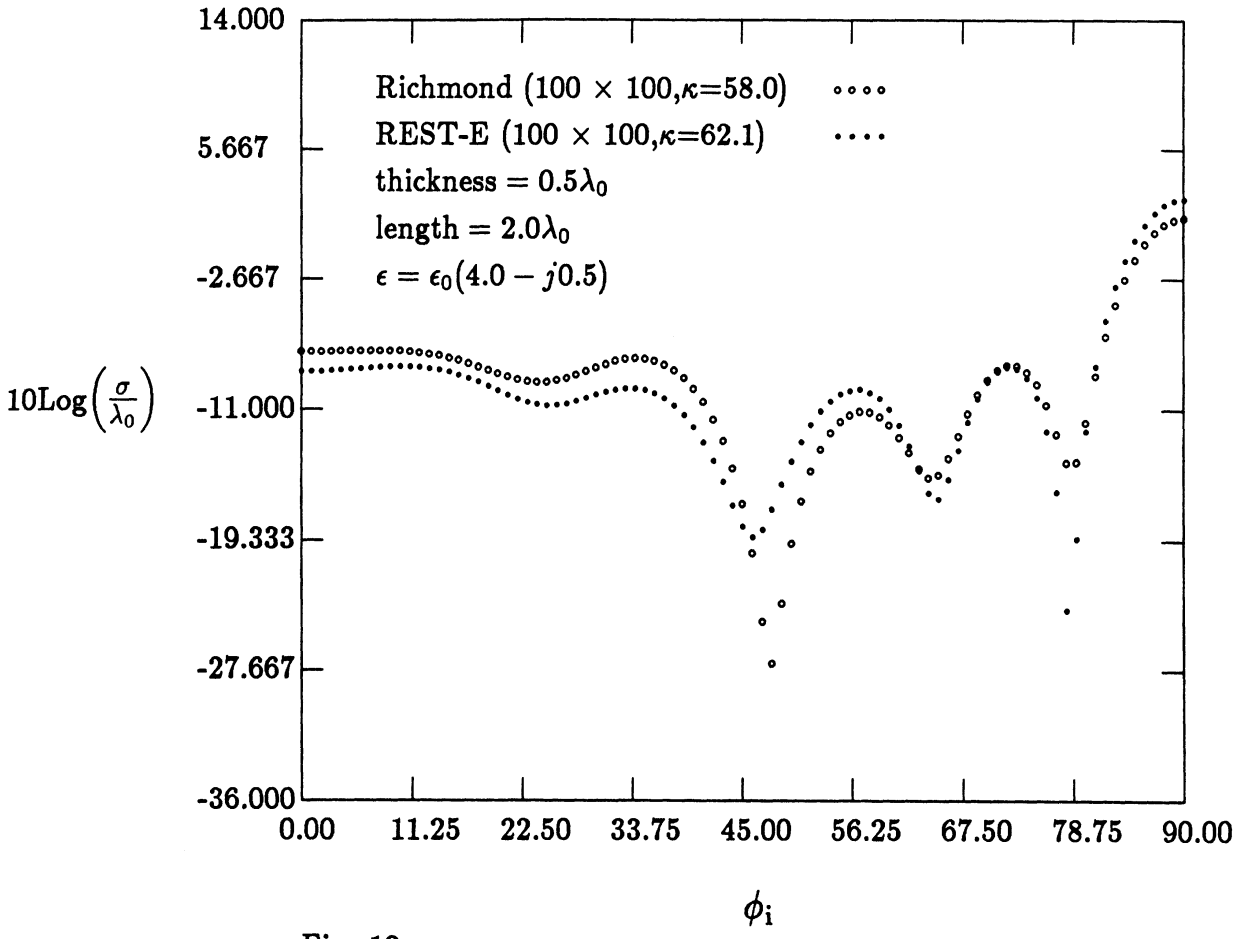
14.000
5.667
-2.667
-11.000
-19.333
-27.667
-36.000
0.00
11.25
22.50
33.75
45.00
56.25
67.50
78.75
90.00
Richmond (100 × 100,κ=58.0)
REST-E (100 × 100,κ=62.1)
thickness = 0.5λ0
length = 2.0λ0
ε = ε0(4.0 − j0.5)
10Log(σ/λ0)
φi

Fig. 13.

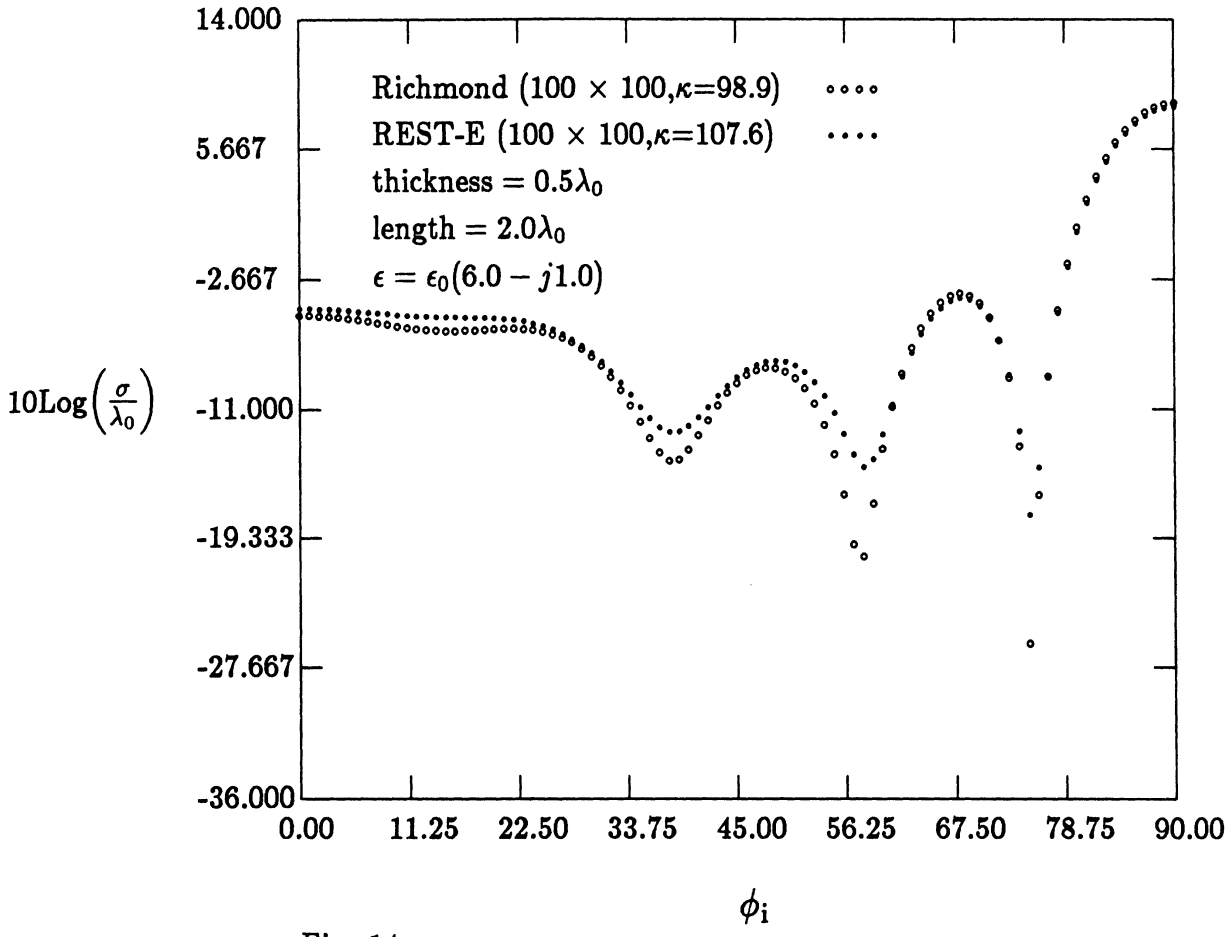
14.000
5.667
-2.667
-11.000
-19.333
-27.667
-36.000
0.00
11.25
22.50
33.75
45.00
56.25
67.50
78.75
90.00
Richmond (100 × 100,κ=98.9)
REST-E (100 × 100,κ=107.6)
thickness = 0.5λ0
length = 2.0λ0
ε = ε0(6.0 − j1.0)
10Log(σ/λ0)
φi

Fig. 14.

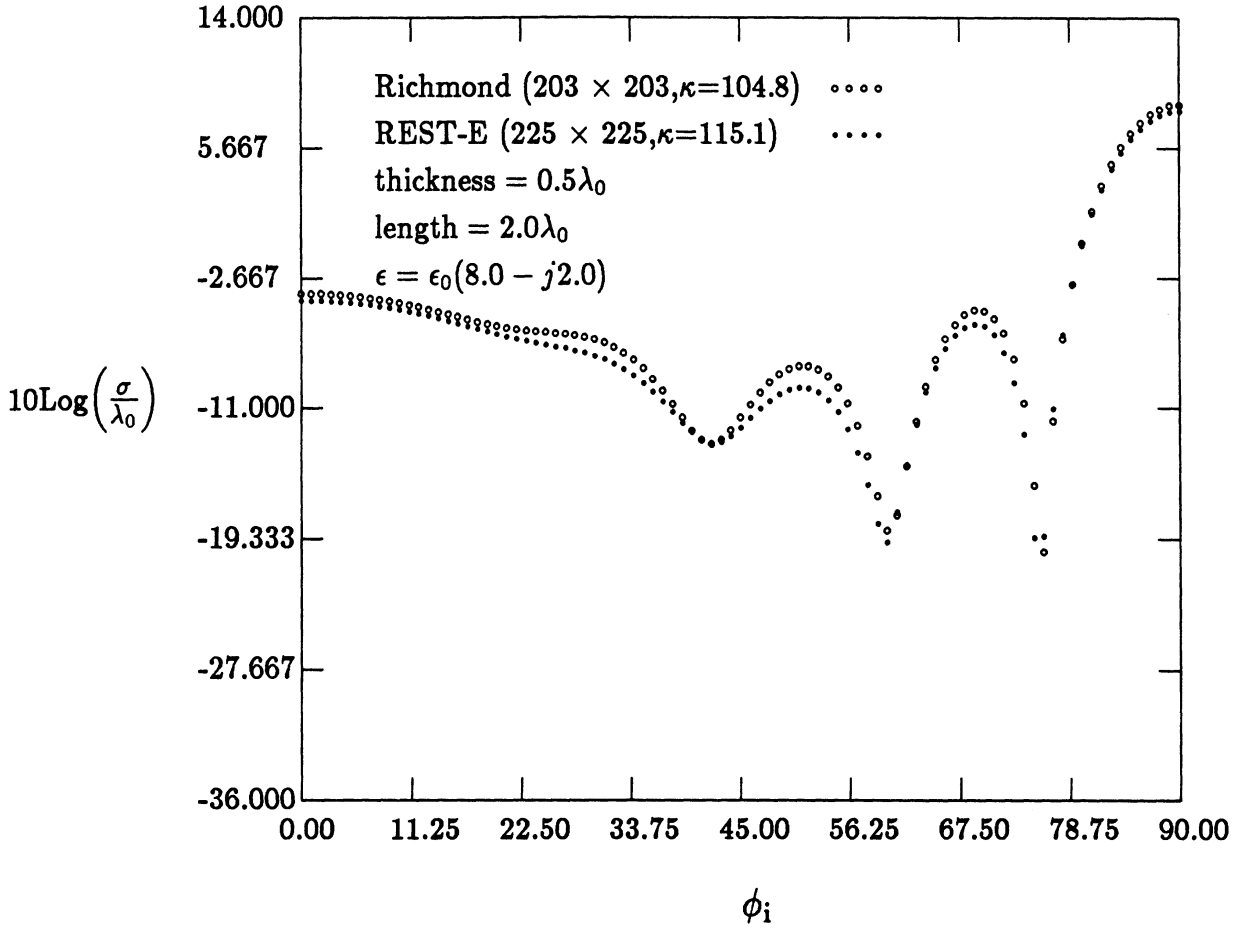
14.000
5.667
-2.667
-11.000
-19.333
-27.667
-36.000
0.00
11.25
22.50
33.75
45.00
56.25
67.50
78.75
90.00
Richmond (203 × 203,κ=104.8)
REST-E (225 × 225,κ=115.1)
thickness = 0.5λ0
length = 2.0λ0
ε = ε0(8.0 − j2.0)
10Log(σ/λ0)
φi

Fig. 15.

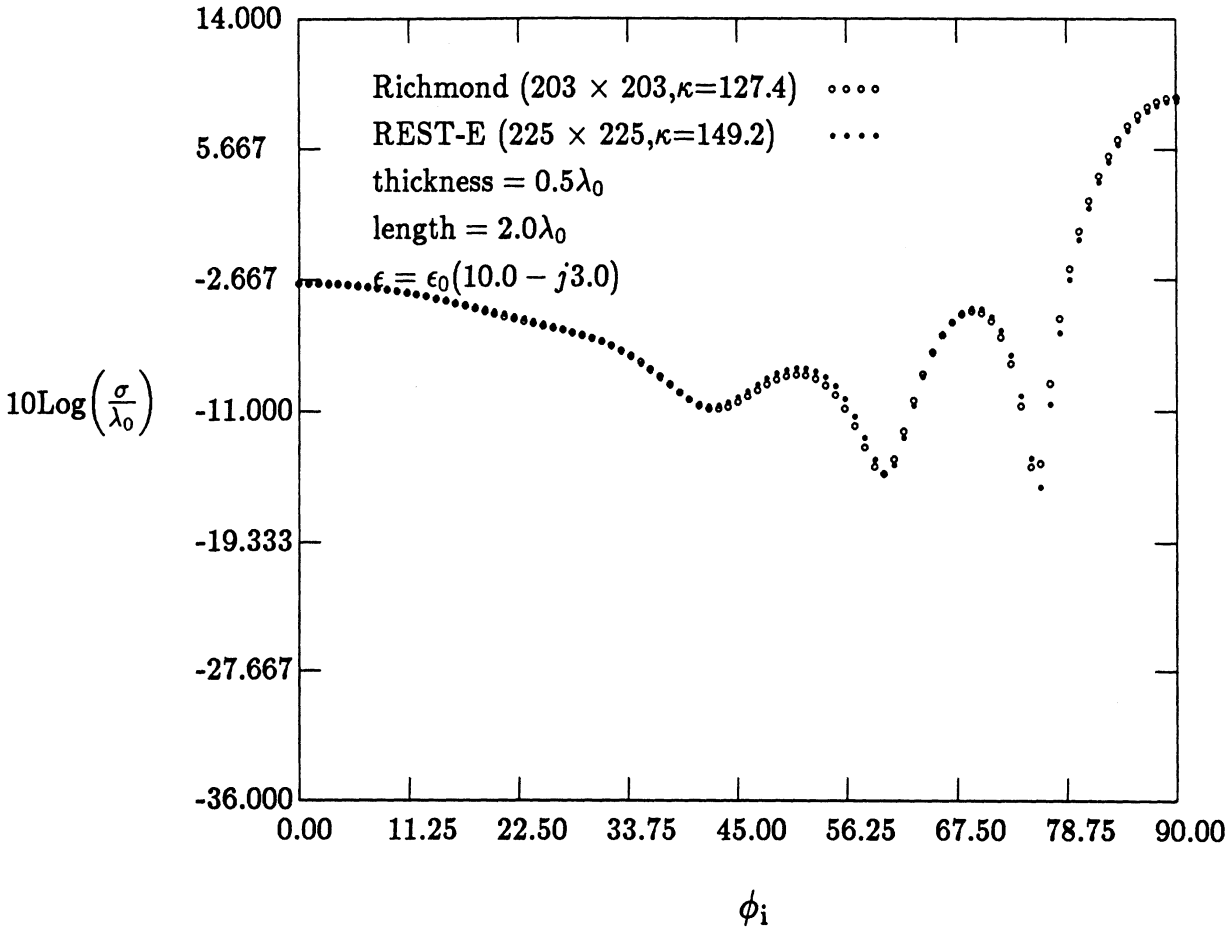
14.000
5.667
-2.667
-11.000
-19.333
-27.667
-36.000
0.00
11.25
22.50
33.75
45.00
56.25
67.50
78.75
90.00
Richmond (203 × 203,κ=127.4)
REST-E (225 × 225,κ=149.2)
thickness = 0.5λ0
length = 2.0λ0
ε = ε0(10.0 − j3.0)
10Log(σ/λ0)
φi

Fig. 16.

References

[1] J. H. Richmond, "Scattering by a Dielectric Cylinder of Arbitrary Cross Section Shape",, IEEE Trans. Antennas Propagat., vol. AP-13,No. 3 ,May, 1965, pp. 334-341.

[2] T. J. Peters, "Radar Cross Section for Stacked Resistive Strips" ,Radiation Laboratory, The University of Michigan,Internal Memo No. 389055-001-M,March 28,1986.

[3] W. D. Burnside, K. W. Burgener, "High Frequency Scattering By a Thin Lossless Dilectric Slab", IEEE Trans. Antennas Propagat., vol. AP-31,No. 1 ,Jan, 1983.

[4] R. F. Harrington, J. R. Mautz, "An Impedance Sheet Approximation for Thin Dielectric Shells", IEEE Trans. Antennas Propagat., vol. AP-23,No. 4 ,July, 1975.

Appendix B - Thick Dielectric Slab REST-H vs Volume I.E.

We have demonstrated in Appendix A that in the case of E_z incidence an inhomogeneous dielectric cylinder can be effectively modeled by stacks (layers) of resistive sheets. The same model can again be employed for the case of H_z incidence. The integral equation (I.E.) for the resistive sheet model is now given by

$$4\frac{Z_s(x,y)}{Z_0}K_l(x,y) + \frac{\partial}{\partial n}\int_{l'}(\hat{n}'\cdot\hat{\rho})K_{l'}(x',y')H_1^{(2)}(k_0\rho)dl' = \frac{4}{Z_0}E_l^i(x,y) \qquad (1)$$

where $\rho = \sqrt{(x-x')^2+(y-y')^2}$, K_l is the surface current flowing in the direction tangent to the sheet and perpendicular to the z axis and $\hat{n}'$ denotes the normal to the sheet. The resistivity $R(l) = Z_s(l)$ was derived in Appendix A, i.e. it is the same as that for the E_z case.

The corresponding (coupled) Volume integral equations are

$$\frac{4k_0}{Z_0}E_x(x,y) - \frac{\partial}{\partial y}\iint_{S'}\left[J_x(x',y')\frac{\partial}{\partial y} - J_y(x',y')\frac{\partial}{\partial x}\right]H_0^{(2)}(k_0\rho)dS' = \frac{4k_0}{Z_0}E_x^i(x,y) \qquad (2)$$

$$\frac{4k_0}{Z_0}E_y(x,y) + \frac{\partial}{\partial x}\iint_{S'}\left[J_x(x',y')\frac{\partial}{\partial y} - J_y(x',y')\frac{\partial}{\partial x}\right]H_0^{(2)}(k_0\rho)dS' = \frac{4k_0}{Z_0}E_y^i(x,y) \qquad (3)$$

where

$$J_{x,y}(x',y') = j\frac{k_0}{Z_0}\left(\epsilon_r(x',y') - 1 - j\frac{\sigma(x',y')}{\omega\epsilon_0}\right)E_{x,y}(x',y'). \qquad (4)$$

Equation (1) is implemented in the code REST-H whereas (2) and (3) are implemented in the code RICH-TE.

Figures 1-4 present a comparison of the results obtained via the REST-H and RICH-TE codes for a number of backscatter and bistatic patterns. Unlike the E_z case, it is seen that the results via the above two formulations differ away from the specular region. This holds, not only for the thick slab but also for the strips of width $\frac{\lambda_0}{10}$. Certainly for sufficiently lossy material (see Fig. 3.) the agreement between the two solutions is reasonable.

The major reason for the inaccuracy of the REST-H code is its inability to model components of the current which may flow normal to the strip. Such components, although absent for the E_z case, are possible for H_z incidence. This is easily recognized by noting that (2) and (3) are equivalent to

$$4\eta(x,y)K_l(x,y) + \frac{\partial}{\partial n}\int_{l'}\left[(\hat{n}'\cdot\hat{\rho})K_{l'}(x',y') + (\hat{l}'\cdot\hat{\rho})K_{n'}(x',y')\right]H_1^{(2)}(k_0\rho)dl' = \frac{4}{Z_0}E_l^i(x,y) \tag{5}$$

$$-4\eta(x,y)K_n(x,y) - \frac{\partial}{\partial l}\int_{l'}\left[(\hat{n}'\cdot\hat{\rho})K_{l'}(x',y') + (\hat{l}'\cdot\hat{\rho})K_{n'}(x',y')\right]H_1^{(2)}(k_0\rho)dl' = \frac{4}{Z_0}E_n^i(x,y) \tag{6}$$

where

$$\eta(x,y) = \frac{-j}{\left(\epsilon_r(x,y) - 1 - j\frac{\sigma(x,y)}{\omega\epsilon_0}\right)k_0 d}. \tag{7}$$

E_l^i and E_n^i are the tangential and normal components of the incident field, respectively at each point of the layer, and K_l and K_n denote the sheet currents flowing tangentially and normal to the layer. Equations (5) - (6) were obtained

from (2) - (3) after integrating out the y-dependence and then generalizing the result to strips (layers) of arbitrary shape. Clearly, (5) reduces to (1) only when $\mathsf{Kn}(x,y) = 0$, which is not always the case.

We have also found that the exact I.E.'s (2)-(3) or (5)-(6) can be related to the coupled boundary conditions given by equations (2) and (9) of the main text. To prove this we begin by noting that (5) and (6) implement the relations

$$E_l = RK_l \tag{8}$$

$$E_n = -RK_n \tag{9}$$

where $E_{l,n}$ denote the total electric field components on the surface of the sheet. Clearly, (7) is the same as (2) in the main text. First, we note that K_n can be replaced by an equivalent magnetic current

$$\bar{M} = \hat{z}\frac{1}{j\omega\epsilon_0\left(\epsilon_r - j\frac{\sigma}{\omega\epsilon_0}\right)}\frac{\partial K_n}{\partial l} = \hat{z}M_z \tag{10}$$

differentiating (9) and making use of (10) yields

$$\frac{\partial E_n}{\partial l} = -j\omega\epsilon_0\left(\epsilon_r - j\frac{\sigma}{\omega\epsilon_0}\right)RM_z \tag{11}$$

which is identical to (9) of the main text.

Based on the results of figures 1-4 and the discussion above, it is concluded that one cannot neglect the boundary condition given in (9) or (11) above, unless the material loss tangent is significant. However, the strip or layer formulation remains acceptable for the H_z case as suggested by the form of (5)-(6). The numerical implementation of these integral equations is currently being considered.

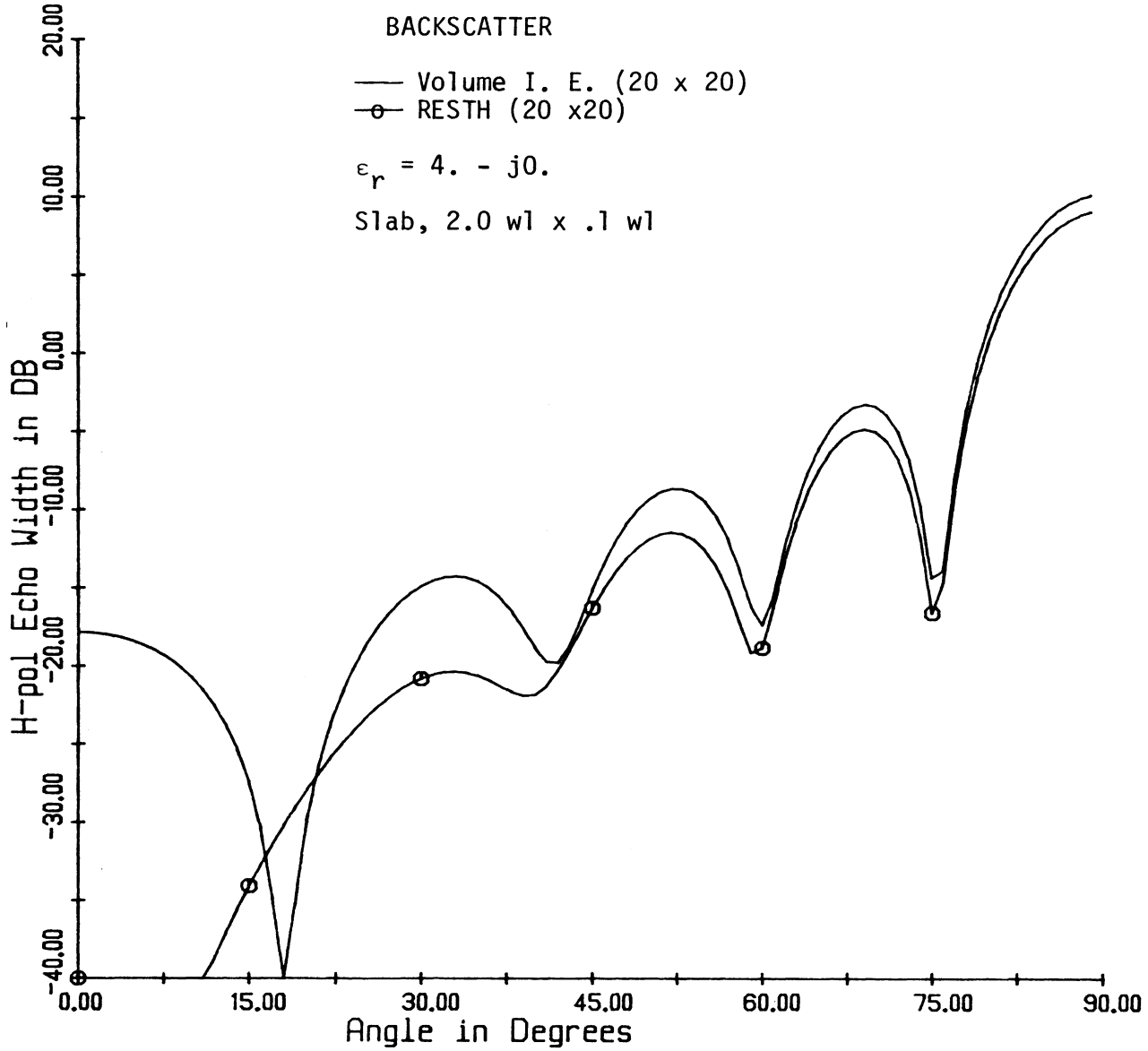
BACKSCATTER
Volume I. E. (20 x 20)
RESTH (20 x20)
ε_r = 4. - j0.
Slab, 2.0 wl x .1 wl
H-pol Echo Width in DB
20.00
10.00
0.00
-10.00
-20.00
-30.00
-40.00
0.00
15.00
30.00
45.00
60.00
75.00
90.00
Angle in Degrees

Figure 1

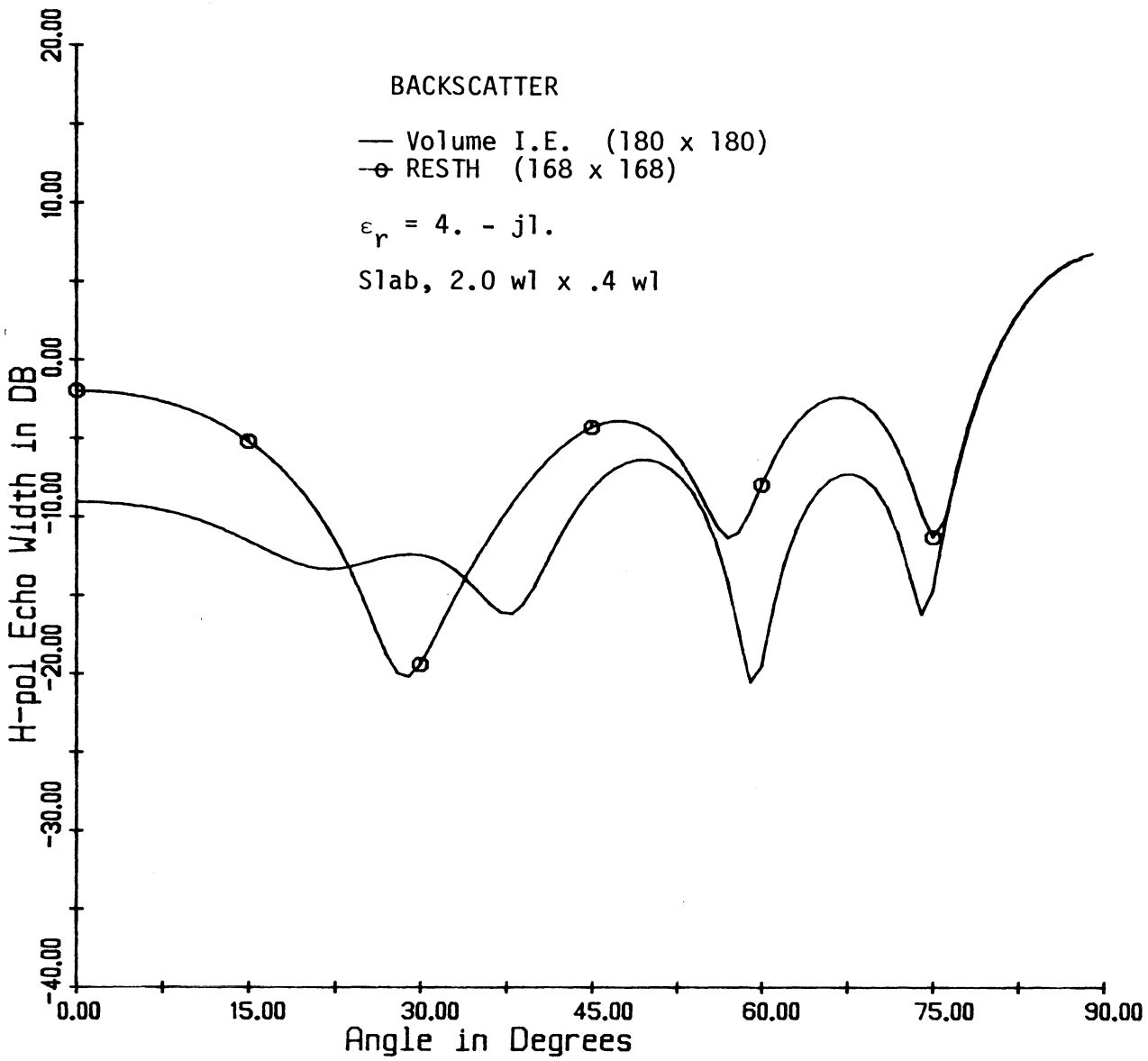
BACKSCATTER
Volume I.E. (180 x 180)
RESTH (168 x 168)
ε_r = 4. - j1.
Slab, 2.0 wl x .4 wl
H-pol Echo Width in DB
20.00
10.00
0.00
-10.00
-20.00
-30.00
-40.00
0.00
15.00
30.00
45.00
60.00
75.00
90.00
Angle in Degrees

Figure 2

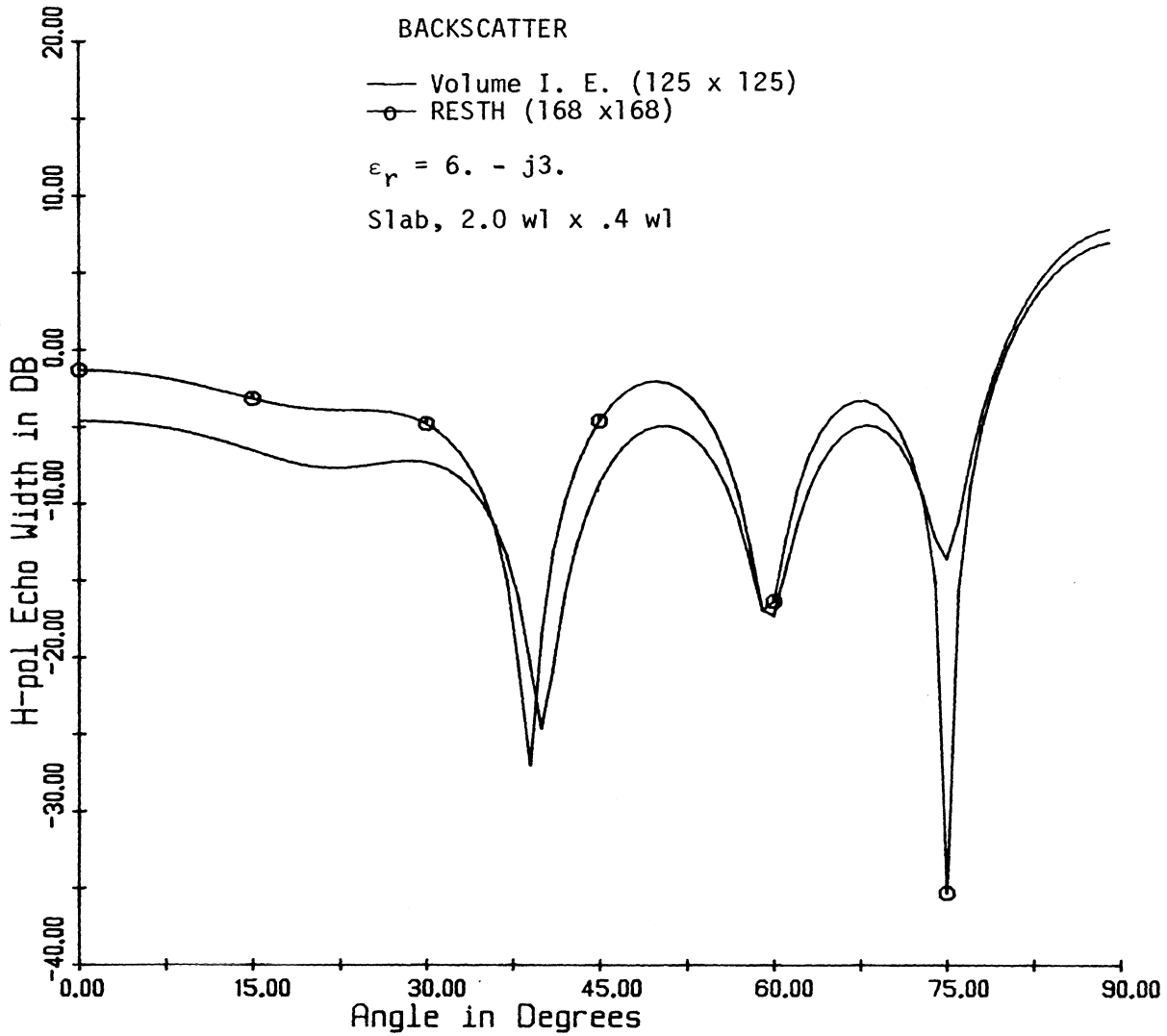
BACKSCATTER
Volume I. E. (125 x 125)
RESTH (168 x168)
ε_r = 6. - j3.
Slab, 2.0 wl x .4 wl
H-pol Echo Width in DB
20.00
10.00
0.00
-10.00
-20.00
-30.00
-40.00
0.00
15.00
30.00
45.00
60.00
75.00
90.00
Angle in Degrees

Figure 3

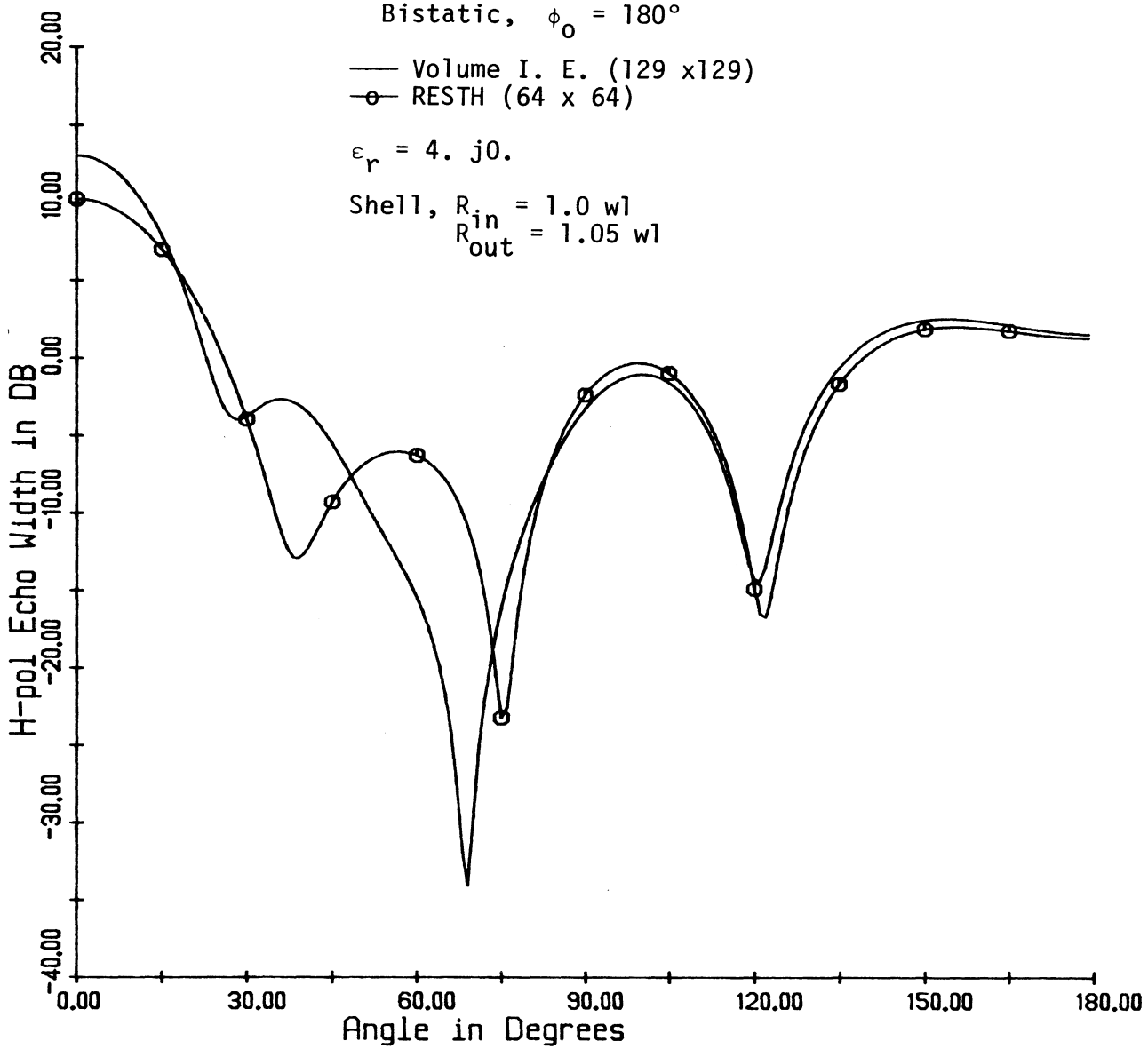
Bistatic, ϕ_o = 180°
Volume I. E. (129 x129)
RESTH (64 x 64)
ε_r = 4. j0.
Shell, R_{in} = 1.0 wl
R_{out} = 1.05 wl
H-pol Echo Width in DB
20.00
10.00
0.00
-10.00
-20.00
-30.00
-40.00
0.00
30.00
60.00
90.00
120.00
150.00
180.00
Angle in Degrees

Figure 4

APPENDIX C

Modifications included in the new versions of

RESTE and RESTH

(April 1986 Versions)

These programs, as did the previous versions (June 1985), numerically solve the problem of an E- and H-polarized plane wave incident at normal incidence on two-dimensional geometry consisted of resistive sheets. These new versions have the added capability which allows:

(a) placement of sheets close together

(b) joining of the sheets to form the junction

The previous versions of the programs were known to produce unreliable results when geometries contained junctions and sheets spaced close together.

The programs are based on the integral equations

$$Y_0 E_z^i(s) = R(s)J_z(s) + \frac{k}{4}\int_C J_z(s')H_0^{(1)}(kr)ds' \qquad (C.1)$$

for E-polarization case, and

$$Y_0 E_s^i(s) = R(s)J_s(s) + \lim_{\rho\to\rho'} \frac{1}{4}\frac{\partial}{\partial n'}\int J_s(s')(\hat{n}'\cdot\hat{r})H_1^{(1)}(kr)\,ds' \qquad (C.2)$$

for H-polarization case. The notation used here is the same as that used by Knott and Senior [1974] when they derived the equations and by Liepa et al. [1974] where the equations were used in development of a generalized two-dimensional program called RAMVS. These equations are also given in Appendices A and B of this report.

For programming purposes equations (C.1) and (C.2) are rewritten as

$$Y_0 E_z^i(s) = A\, J_z(s) \qquad \text{for E-polarization} \qquad (C.2)$$

and $$Y_0 E_z^i(s) = B\, J_z(s) \qquad \text{for H-polarization} \qquad (C.3)$$

where $$A\, J_z(s) = \left\{ R(s) + \frac{\delta}{\lambda} \left[\frac{\pi}{2} + i \left(\ell n \frac{\delta}{\lambda} + 0.02879837 \right) \right] \right\}_{\delta} J_z(s) \qquad (C.4)$$

$$+ \frac{1}{4} \int_{C-\delta} J_z(s') H_0^{(1)}(kr) d(ks')$$

and

$$BJ_s(s) = R(s) + \frac{\pi}{4} \left(\frac{\delta}{\lambda}\right) + i \frac{1}{2} \left\{ \frac{2}{\pi^2 \left(\frac{\delta}{\lambda}\right)} + \frac{\delta}{\lambda} \left(1n \frac{\delta}{\lambda} - 0.47120163 \right) \right\} J_s(s) \qquad (C.5)$$

$$+ \frac{1}{4} \int_{C-\delta} J_s(s') \left\{ (\hat{n}' \cdot \hat{n}) H_0^{(1)}(kr) + \frac{\partial}{\partial (ks')} \left[(\hat{s} \cdot \hat{r}) H_1^{(1)}(kr) \right] \right\} d(ks')$$

The first terms in the above equations represent the self-cell contributions obtained by integrating over the singularities (see Appendices D and E), and the integrals represent contributions over the remainder of the body.

The programs RESTE and RESTH are two self-standing codes appropriate for E-polarization and H-polarization cases, respectively. Each program consists of a main program and the same subroutine package RSUBS that generates the geometry, the matrix, solves the matrix, etc. The codes are written in FORTRAN and are self-contained, requiring only the basic system-supplied functions.

The codes employ pulse basis functions or representation of the current on the body, matching the boundary condition at the center of the pulse. This is accomplished by subdividing the code in small increments (cells), each prescribed by the start point a(δ), the centerpoint, and the endpoint b(δ). The normal derivatives at these points are also computed. Subroutine GEOM (in RSUBS package) generates

the above data.

Subroutines MTXE and MTXH generate the matrix elements from equations (C.4) and (C.5), respectively. In MTXE the matrix elements are computed using

$$Q_{ij} = R_i + \frac{\delta_j}{\lambda}\left[\frac{\pi}{2} + i\left(\ell n \frac{\delta_j}{\lambda} + 0.02879837\right)\right], \quad i = j \qquad (C.6)$$

$$= \frac{\pi}{2}\int_{S_j} H_0^{(1)}(kr)\,d\left(\frac{\delta_j}{\lambda}\right), \quad i \neq j$$

and in MTXH using

$$b_{ij} = R_i + \frac{\pi}{4}\left(\frac{\delta j}{\lambda}\right) + j\frac{1}{2}\left\{\frac{2}{\pi^2\left(\frac{\delta_j}{\lambda}\right)} + \frac{\delta_j}{\lambda}\left(\ell n \frac{\delta_j}{\lambda} - 0.47120163\right)\right\}, \quad i = j \qquad (C.7)$$

$$= \frac{\pi}{2}\int_{S_j} (\hat{n}_j \cdot \hat{n}_i) H_0(kr)\,d\left(\frac{\delta_j}{\lambda}\right) + \frac{1}{4}(\hat{s}_i \cdot \hat{r}) H_1^{(1)}(kr)\Bigg|_{a_i}^{b_j}, \quad i \neq j$$

where $\underline{r} = \underline{r}_j - \underline{r}_i$. The subscript j designates the source point and subscript i designates the observation or matching point. The last term in (C.7) is obtained by recognizing the exact integral form in (C.5) and as long as the current J_s is constant over the range of integration (the cell), the above representation is valid. The self-cell terms (i = j) are evaluated exactly as shown in (C.6) and (C.7) but the integral terms are evaluated using three- and five-point Simpson's rules, viz.

$$\int_{a_j}^{b_j} f(x)\,dx = \frac{\delta_j}{6}\left(f(1) + 4f(2) + f(3)\right) \qquad (C.8)$$

and

$$= \frac{\delta_j}{90}\left(7f(1) + 32f(12) + 12f(2) + 32f(23) + 7f(3)\right) \qquad (C.9)$$

respectively. The quantity δ_j in the cell length, $\delta_j = b_j - a_j$, and the argument 1,2,3 for the f's designate the start, the center, and the end points on the cell respectively. In equation (C.9) arguments 12 and 23 represent points halfway between 1 and 2 and 2 and 3 respectively.

In computations, normally the three-point evaluations are used, except when $|r| < \delta$, which can occur when the sheets are spaced less than δ apart or when they join at a point to form a junction. For the last case the five-point evaluations are used. Since subroutine GEOM generates only the starting, the center, and the end point for the cell, subroutine MORPTS is called to provide the additional points needed for the five point evaluations. This subroutine uses the assumed geometry characteristic being either a straight segment (in which case a linear interpolation is used to determine the additional points) or a circular arc (in which case the properties of a circle are used to determine the additional points).

The present versions of RESTE and RESTH were tested by comparing their results with perfectly conducting cylinders and then running ogival cylinders as their thickness approached zero. The most severe test for the programs that we could think is that of two ogival cylinders touching at the vertex as shown in Fig. C1. This geometry tests the ability of the program to handle the junctions and the case when the sheets are extremely close together. For the ogives and the strip shown in Fig. C1, RESTE and RESTH were run with $\delta = 0.082$ and the backscattering results are tabulated in Table C1. The case $\theta = 0^\circ$ corresponds to the edge-on incidence and $\theta = 90^\circ$ to the top incidence. As expected the results for very thin ogives reduce to those for a strip, thus validating the accuracy of the codes. Some 0.2 dB difference can be attributed to the sampling (cell size) used, since for runs with $\delta = 0.03\ \lambda$ the difference decreased to about 0.05 dB.

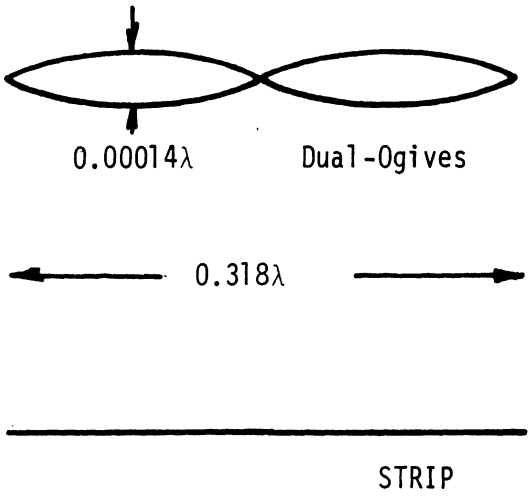

Fig. C1. Models used for testing RESTE and RESTH.

Table C1. Double Ogive Vs. Strip

	(H-POLARIAZATION)		(E-POLARIZATION)	
	OGIVE	STRIP	OGIVE	STRIP
THETA	dB	dB	dB	dB
0.0	-119.58	-500.00	-7.61	-7.43
10.00	-30.00	-30.37	-7.59	-7.40
20.00	-18.13	-18.49	-7.60	-7.40
30.00	-11.35	-11.69	-7.79	-7.57
40.00	-6.62	-6.91	-7.84	-7.68
50.00	-2.79	-2.99	-6.10	-6.06
60.00	0.61	0.49	-2.44	-2.42
70.00	3.43	3.37	0.93	0.98
80.00	5.30	5.27	3.05	3.13
90.00	5.95	5.93	3.76	3.86
100.00	5.30	5.27	3.05	3.13
110.00	3.43	3.37	0.93	0.98
120.00	0.61	0.49	-2.44	-2.42
130.00	-2.79	-2.99	-6.10	-6.06
140.00	-6.62	-6.91	-7.84	-7.68
150.00	-11.35	-11.69	-7.79	-7.57
160.00	-18.13	-18.49	-7.60	-7.40
170.00	-30.00	-30.37	-7.59	-7.40
180.00	-119.58	-232.03	-7.61	-7.43

References

C1 Knott, E.F., and T.B.A. Senior (1974), "Non-Specular Radar Cross Section Study," University of Michigan Radiation Lab Report No. 011764-1-T, and AFAL-TR-73-422.

C2 Liepa, V.V., E.F. Knott, T.B.A. Senior (1974), "Scattering From Two-Dimensional Bodies with Absorber Sheets," University of Michigan Radiation Lab Report No. 011764-2-T and AFAL-TR-74-119.

Appendix D - Solution of the I. E. for Resistive Sheets E-Pol

I. Formulation of Integral Equation

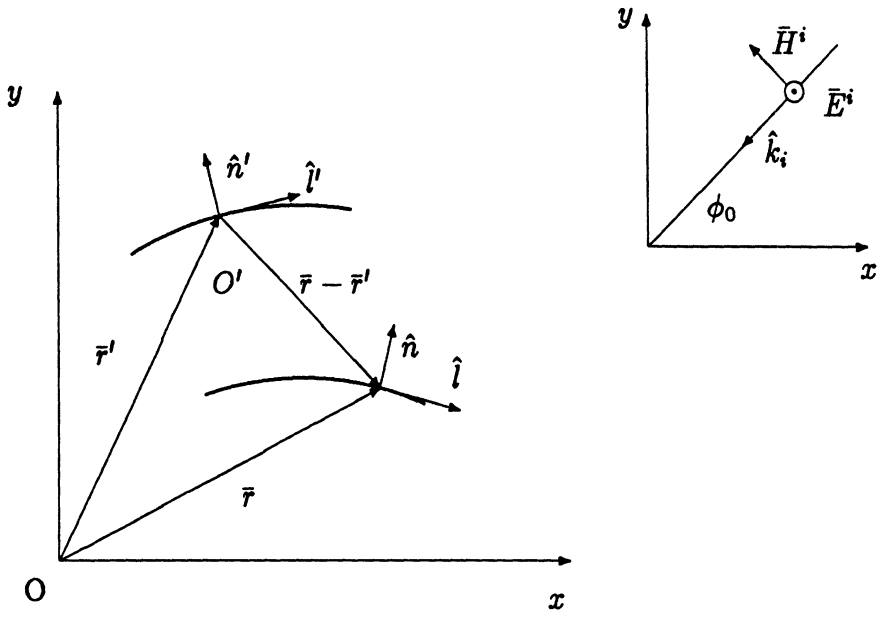

Fig. 1. General multiple strip configuration

The integral equation is formulated by equating the total field to the sum of the incident and scattered fields on the surface of each strip. Assume the $-i\omega t$ time convention is used such that the incident electric and magnetic fields may be described as

$$\bar{E}^i(\bar{r}) = E_{oi}e^{i(\bar{k}_i\cdot\bar{r})}\hat{z} = E_{oi}e^{-ik(xcos(\phi_o)+ysin(\phi_o))}\hat{z} \tag{1}$$

and

$$\bar{H}^i(\bar{r}) = \frac{1}{Z_o}\hat{k}_i \times \bar{E}^i(\bar{r}) \tag{2}$$

where $k = \omega\sqrt{\mu_0\epsilon_0}$ is the freespace wave number, $Z_0 = \sqrt{\frac{\mu_0}{\epsilon_0}}$ is the characteristic wave impedance of free space and ϕ_0 is the angle of incidence. The induced electric current has only a z component and is assumed to vary only along the width of each strip.

$$\bar{K} = K_z(x,y)\hat{z} \tag{3}$$

From [1] define a Hertz vector of the electric kind as

$$\bar{\Pi}(\bar{R}) = \frac{iZ_o\hat{z}}{4\pi k}\int_{l'}\int_{-\infty}^{\infty} K_z(x',y')\frac{e^{ik\sqrt{(x-x')^2+(y-y')^2+(z-z')^2}}}{\sqrt{(x-x')^2+(y-y')^2+(z-z')^2}}dz'dl'. \tag{4}$$

where

$$\bar{E}(\bar{R}) = \nabla\times\nabla\times\bar{\Pi}(\bar{R}) \tag{5}$$

$$\bar{H}(\bar{R}) = -i\frac{k}{Z_0}\nabla\times\bar{\Pi}(\bar{R}) \tag{6}$$

and $\bar{\Pi}$ satisfies the differential equation

$$\nabla^2\bar{\Pi}(\bar{R}) + k^2\bar{\Pi}(\bar{R}) = -\frac{i}{\omega\epsilon_0}\bar{J}(\bar{R}'). \tag{7}$$

The following integral identity reduces the formulation to two dimensions.

$$\int_{-\infty}^{\infty} \frac{e^{ik\sqrt{(x-x')^2+(y-y')^2+(z-z')^2}}}{\sqrt{(x-x')^2+(y-y')^2+(z-z')^2}} dz' = i\pi H_0^{(1)}\left(k\sqrt{(x-x')^2+(y-y')^2}\right) \tag{8}$$

The two dimensional Hertz vector is expressed as

$$\bar{\Pi}(x,y) = \frac{-Z_o\hat{z}}{4k}\int_{l'} K_z(x',y')H_0^{(1)}\left(k\sqrt{(x-x')^2+(y-y')^2}\right) dl'. \tag{9}$$

Since $\bar{\Pi}$ has only a z component which is not a function of z, the electric field may be written as

$$\bar{E}(\bar{r}) = k^2\bar{\Pi}(\bar{r}). \tag{10}$$

The scattered electric field will be of the form

$$\bar{E}^s(x,y) = \frac{-kZ_0\hat{z}}{4}\int_{l'} K_z(x',y')H_0^{(1)}\left(k\sqrt{(x-x')^2+(y-y')^2}\right) dl'. \tag{11}$$

The total tangential electric field on the surface of each strip is equal to the sum of the incident plus the scattered tangential components.

$$E_z^t(x,y) = E_z^i(x,y) - \frac{kZ_o}{4}\int_{l'} K_z(x',y')H_0^{(1)}\left(k\sqrt{(x-x')^2+(y-y')^2}\right) dl' \tag{12}$$

In order to solve the equation, the boundary condition on the surface of each strip must be postulated.

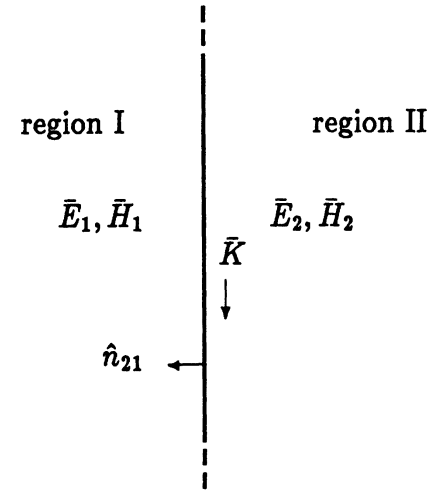

Fig. 2. Boundary of resistive strip

$$\hat{n}_{21} \times (\bar{E}_1 - \bar{E}_2) = 0 \tag{13}$$

$$\hat{n}_{21} \times (\bar{H}_1 - \bar{H}_2) = \bar{K} = \frac{\bar{E}_1 - (\hat{n}_{21} \cdot \bar{E}_1)\hat{n}_{21}}{R} = \frac{\bar{E}_2 - (\hat{n}_{21} \cdot \bar{E}_2)\hat{n}_{21}}{R} \tag{14}$$

$$\hat{n}_{21} \times (\bar{D}_1 - \bar{D}_2) = \rho_s = \frac{1}{i\omega} \nabla \cdot \bar{K} \tag{15}$$

$$\hat{n}_{21} \times (\bar{B}_1 - \bar{B}_2) = 0 \tag{16}$$

Observation of (14) shows that the total tangential electric field may be related to the surface resistance and the surface current. For convenience, define the resistance normalized to the freespace impedance as $\eta = \frac{R}{Z_0}$.

$$E_z = Z_0 \eta K_z. \tag{17}$$

Substituting (17) into (12) yields an integral equation enforced on the surface of each strip.

$$\frac{4}{k}\eta(x,y)K_z(x,y) + \int_{l'} K_z(x',y') H_0^{(1)}\left(k\sqrt{(x-x')^2 + (y-y')^2}\right) dl' = \frac{4}{kZ_0} E_z^i(x,y) \tag{18}$$

II. Solution Using Method of Weighted Residuals

On the surface of the strip define the residual as the sum of the tangential incident and scattered fields minus the total field such that $Residual = E_z^i(l) + E_z^s(l) - E_z^t(l)$. The method of weighted residuals is used to set the integral of a weighting function $w(l)$ times the residual equal to zero. This satisfies the boundary condition in an average sense as opposed to at discrete points. Let each strip be composed of cells with arc length δ and assume the current is approximated by a series of expansion functions with constant coefficients.

$$K(l') = \sum_{q=1}^{N} K(q)L(l') \tag{19}$$

$$L(l') = \begin{cases} h(l') & l_q - \frac{\delta_q}{2} \leq l' \leq l_q + \frac{\delta_q}{2} \\ 0 & \text{otherwise} \end{cases} \tag{20}$$

Equation (18) may be solved discretely by substituting in (19) and integrating both sides with respect to a weight function. Let p denote the integration of the residual times the weighting function over the pth observation cell element. Let q denote the integration of the expansion function times the kernel over the qth source cell element. The system of equations may be written in a compact form as

$$\sum_{p=1}^{N} \left[u(p)K(p) + \sum_{q=1}^{N} f(p,q)K(q) = v(p) \right] \tag{21}$$

where

$$u(p) = \frac{4}{k} \int_{l_p - \frac{\delta_p}{2}}^{l_p + \frac{\delta_p}{2}} w(l)\eta(l)h(l)dl \tag{22}$$

$$v(p) = \frac{4}{kZ_0} \int_{l_p - \frac{\delta_p}{2}}^{l_p + \frac{\delta_p}{2}} w(l)E_z^i(l)dl \tag{23}$$

$$f(p,q) = \int_{l_p-\frac{\delta_p}{2}}^{l_p+\frac{\delta_p}{2}} w(l) \left[\int_{l_q-\frac{\delta_q}{2}}^{l_q+\frac{\delta_q}{2}} h(l')g(l,l')dl' \right] dl \tag{24}$$

and

$$g(l,l') = H_0^{(1)}\left(k\sqrt{(x-x')^2+(y-y')^2}\right). \tag{25}$$

III. Application to Parallel Stacked Resistive Strips

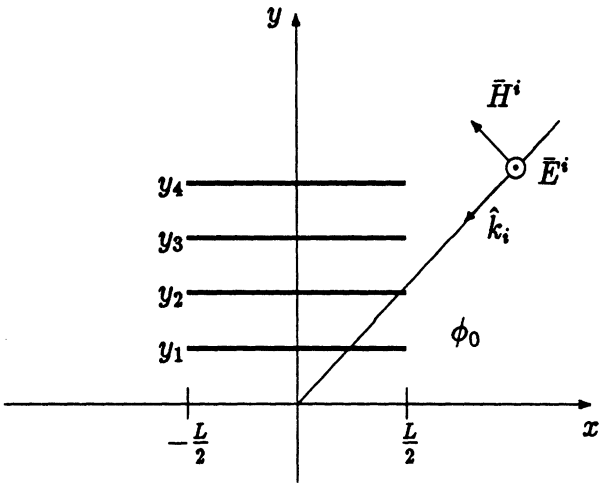

Fig. 3. Geometry of stacked resistive strips

The simplest representative case of multiple resistive strips is shown in Fig. 3. Let δ be the cell width and N the total number of cells.

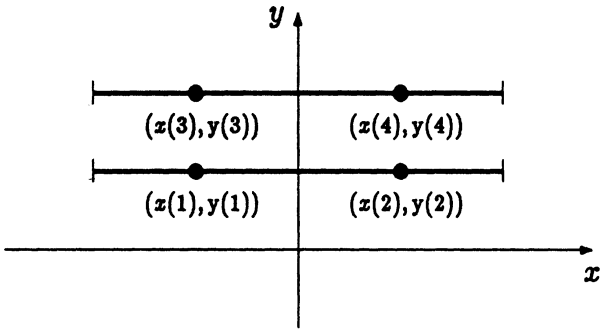

Fig. 4. Two strips with a total of 4 cells

The matrix form of (21) for the geometry shown in Fig. 4 is written as

$$\begin{bmatrix} u_1 + f_{11} & f_{12} & f_{13} & f_{14} \\ f_{21} & u_2 + f_{22} & f_{23} & f_{24} \\ f_{31} & f_{32} & u_3 + f_{33} & f_{34} \\ f_{41} & f_{42} & f_{43} & u_4 + f_{44} \end{bmatrix} \begin{bmatrix} K_1 \\ K_2 \\ K_3 \\ K_4 \end{bmatrix} = \begin{bmatrix} v_1 \\ v_2 \\ v_3 \\ v_4 \end{bmatrix} \tag{26}$$

Observation of (26) shows that the surface resistance and the self cell contributions are the diagonal elements of the matrix.

Assume that the expansion function is a pulse and the weighting function is a delta function.

$$h(l') = h(x', y') = \begin{cases} 1 & x_q - \frac{\delta}{2} \leq x' \leq x_q + \frac{\delta}{2} \quad y' = \text{constant} \\ 0 & \text{otherwise} \end{cases} \tag{27}$$

$$w(l) = w(x, y) = \begin{cases} \delta(x - x_p) & x_p - \frac{\delta}{2} \leq x \leq x_p + \frac{\delta}{2} \quad y = \text{constant} \\ 0 & \text{otherwise} \end{cases} \tag{28}$$

$$g(l, l') = g(x, y, x', y') = H_0^{(1)}\left(k\sqrt{(x - x')^2 + (y - y')^2}\right) \tag{29}$$

$$f(p, q) = \int_{x_q - \frac{\delta}{2}}^{x_q - \frac{\delta}{2}} H_0^{(1)}\left(k\sqrt{(x_p - x')^2 + (y_p - y_q)^2}\right) dx' \tag{30}$$

Case I - non-singular integrand

If cell(p)≠cell(q) and $|y_p - y_q| \geq \delta$ then the observation point is greater than or equal to one cell length away from the source point. Simpson's three point composite rule is used to numerically solve for $f(p, q)$. Each cell interval δ is broken up into $2M$ subintervals.

$$\int_a^b f(x)dx = \frac{h}{3}\left[f(a) + 2\sum_{n=1}^{M-1} f(x_{2n}) + 4\sum_{n=1}^{M} f(x_{2n-1}) + f(b)\right] \tag{31}$$

where

$$h = \frac{b-a}{2M} \tag{32}$$

$$x_{2n} = a + 2nh \tag{33}$$

and

$$x_{2n-1} = a + (2n-1)h. \tag{34}$$

Thus

$$\begin{aligned} f(p,q) &= \frac{h}{3}\left[g\left(x_p, y_p, x_q - \frac{\delta}{2}, y_q\right) + g\left(x_p, y_p, x_q + \frac{\delta}{2}, y_q\right)\right] \\ &\quad +2\frac{h}{3}\left[\sum_{n=1}^{M-1} g(x_p, y_p, x_{q2n}, y_q) + 2\sum_{n=1}^{M} g(x_p, y_p, x_{q(2n-1)}, y_q)\right] \end{aligned} \tag{35}$$

where

$$h = \frac{\delta}{2M} \tag{36}$$

$$x_{q2n} = x_q - \frac{\delta}{2} + 2nh \tag{37}$$

and

$$x_{q(2n-1)} = x_q - \frac{\delta}{2} + (2n-1)h. \tag{38}$$

Case II - singular integrand

If cell(p)=cell(q) or $|y_p - y_q| \leq \delta$ then the observation point is less than or equal to one cell length away from the source point and the integrand becomes unbounded. The small argument approximation of the Hankel function is then integrated analytically. From [2]

$$H_0^{(1)}(z) = J_0(z) + iN_0(z) \tag{39}$$

where

$$J_0(z) = \sum_{m=0}^{\infty} \frac{(-1)^m}{(m!)^2} \left(\frac{z}{2}\right)^{2m} \tag{40}$$

and

$$N_0(z) = \frac{2}{\pi}\left(ln\left(\frac{z}{2}\right) + \gamma\right) J_0(z) - \frac{2}{\pi} \sum_{m=1}^{\infty} \frac{(-1)^m}{(m!)^2} \left(\frac{z}{2}\right)^{2m} \sum_{s=1}^{m} \left(\frac{1}{s}\right). \tag{41}$$

Combining (40) and (41) for $m = 0$

$$H_0^{(1)}(z) = 1 + i\frac{2}{\pi}\left[ln\left(\frac{z}{2}\right) + \gamma\right] + O(z^2) \tag{42}$$

where $\gamma = 0.5772157$ is known as Euler's constant. Making the substitution $d = y - y' = y_p - y_q$ (30) may be written as

$$f(p,q) = \delta + i\frac{2\gamma\delta}{\pi} + i\frac{2}{\pi}\int_{x_q-\frac{\delta}{2}}^{x_q+\frac{\delta}{2}} ln\left(\frac{k}{2}\sqrt{(x_p - x')^2 + d}\right) dx'. \tag{43}$$

Letting $t = x_p - x' = x_q - x'$

$$f(p,q) = \delta + i\frac{2\delta\gamma}{\pi} + i\frac{2\delta}{\pi} ln\left(\frac{k}{2}\right) + i\frac{2}{\pi}\int_0^{\frac{\delta}{2}} ln(t^2 + d^2)dt. \tag{44}$$

Using the integral identity

$$\int ln(a^2 + x^2)dx = xln(a^2 + x^2) - 2x + 2atan^{-1}\left(\frac{x}{a}\right) \tag{45}$$

(44) becomes

$$f(p,q) = \delta + i\frac{2\delta}{\pi}\left[ln\left(\frac{k}{4}\sqrt{\delta^2 + 4d^2}\right) + \frac{2d}{\delta} tan^{-1}\left(\frac{\delta}{2d}\right) + \gamma - 1\right]. \tag{46}$$

For $d = 0$ the self cell value is given by

$$f(p,q) = \delta + i\frac{2\delta}{\pi}\left[ln\left(\frac{k\delta}{4}\right) + \gamma - 1\right]. \tag{47}$$

Elements affected by case II occur along the diagonals of the matrix. This may be observed by viewing the matrix derived from the geometry shown in Fig. 5.

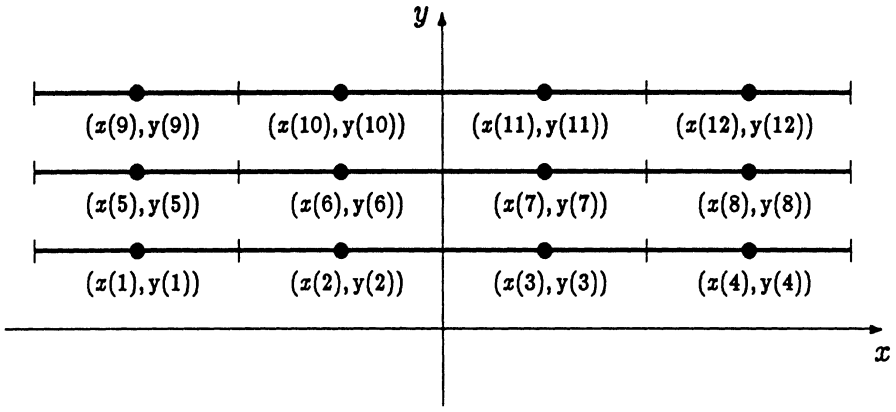

Fig. 5. Three strips with a total of 12 cells

The system of equations for Fig. 5 may be written in matrix form as

$$[S][K] = [V]. \tag{48}$$

If the cell width and resistance are the same and constant for each strip then $[S]$ is a block Toeplitz matrix. This means that $[S]$ and all sub matrices $[S]_{mn}$ are Toeplitz. A Toeplitz matrix is one that is symmetric and all the elements on a particular diagonal are the same.

$$[S] = \begin{bmatrix} [S]_{11} & [S]_{12} & [S]_{13} \\ [S]_{12} & [S]_{11} & [S]_{12} \\ [S]_{13} & [S]_{12} & [S]_{11} \end{bmatrix} \tag{49}$$

The case II terms make up the diagonals of all $[S]_{mn}$ for $m \neq n$ the self cell terms comprise the diagonal elements of $[S]_{mm}$. The distinction between case I and case II becomes critical as $|y_p - y_q| \to 0$ for $x_p = x_q$. If $|y_p - y_q| = d$ then the graph of $|f(p,q)|$ as a function of $\frac{d}{\delta}$ for $0 \leq \frac{d}{\delta} \leq 1$ is given by Fig. 6.

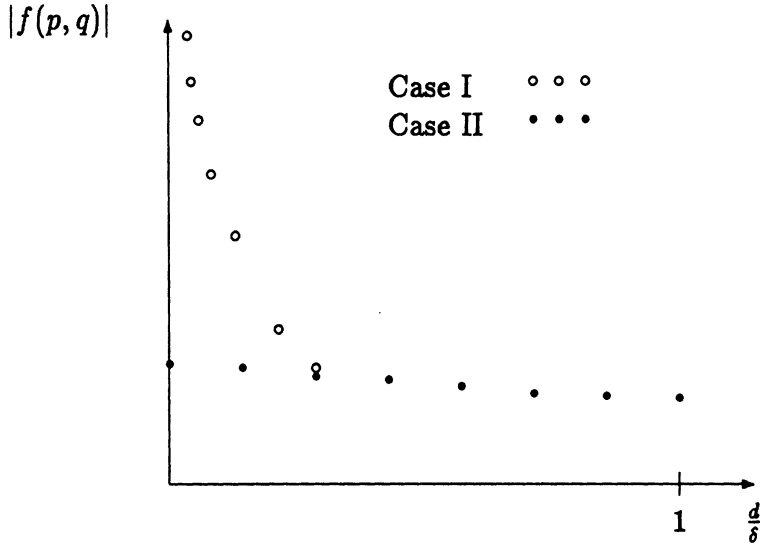

Fig. 6. Matrix elements vs vertical spacing

Fig. 6 shows that case II elements remain finite and approach the self cell value as the spacing between two strips approaches zero compared with case I elements which increase without bound. A more detailed analysis of the data shown in Fig. 6 is given in [5].

IV. Calculation of Scattered Electric Field

The scattered electric field given in (11) may be simplified if the observation is in the far field such that $r >> r'$.

$$\bar{E}^s(\bar{r}) = -\frac{kZ_0}{4}\hat{z}\int_{l'} K_z(\bar{r}')H_0^{(1)}(k|\bar{r}-\bar{r}'|)dl' \tag{50}$$

where

$$H_0^{(1)}(k|\bar{r}-\bar{r}'|) = \sqrt{\frac{2}{\pi k}}e^{-i\frac{\pi}{4}}\frac{e^{ik|\bar{r}-\bar{r}'|}}{|\bar{r}-\bar{r}'|}. \tag{51}$$

In the far zone (51) is simplified by assuming

$$|\bar{r}-\bar{r}'| = \begin{cases} r-\hat{r}\cdot\bar{r}' & \text{numerator} \\ \\ r & \text{denominator} \end{cases} \tag{52}$$

such that

$$H_0^{(1)}(k|\bar{r}-\bar{r}'|) = \sqrt{\frac{2}{\pi kr}}e^{-i\frac{\pi}{4}}e^{ikr}e^{-ik(x'cos(\phi)+y'sin(\phi)}. \tag{53}$$

Substituting (53) into (50)

$$\begin{aligned} \bar{E}^s(\phi) &= -\hat{z}Z_0e^{-i\frac{\pi}{4}}\frac{e^{ikr}}{\sqrt{r}}\sqrt{\frac{k}{8\pi}}\int_{l'}K_z(x',y')e^{-ik(x'cos(\phi)+y'sin(\phi))}dl'. \\ &= -\hat{z}Z_0e^{-i\frac{\pi}{4}}\frac{e^{ikr}}{\sqrt{r}}\sqrt{\frac{k}{8\pi}}\sum_{q=1}^{N}K_z(q)e^{-iky_qsin(\phi)}\int_{x_q-\frac{\delta}{2}}^{x_q+\frac{\delta}{2}}e^{-ikx'cos(\phi)}dx' \\ &= -\hat{z}Z_0\delta e^{-i\frac{\pi}{4}}\frac{e^{ikr}}{\sqrt{r}}\sqrt{\frac{k}{8\pi}}\sum_{q=1}^{N}K_z(q)e^{-ik(x_qcos(\phi)+y_qsin(\phi))}. \end{aligned} \tag{54}$$

V. Calculation of Radar Cross Section

The radar cross section σ is defined as

$$\begin{aligned} \sigma &= \lim_{r\to\infty}\left[2\pi r\frac{|\bar{E}^s|^2}{|\bar{E}^i|^2}\right] \\ &= \frac{k}{4}(\delta Z_0)^2\left|\sum_{q=1}^{N}K_z(q)e^{-ik(x_qcos(\phi)+y_qsin(\phi))}\right|^2. \end{aligned} \tag{55}$$

REFERENCES

[1] J. A. Stratton, Electromagnetic Theory. New York: McGraw-Hill, 1941, pp. 430-431.

[2] P. M. Morse and H. Feshbach, Methods of Theoretical Physics. New York: McGraw-Hill, 1953, Part I, p. 627.

[3] E. F. Knott and T. B. A. Senior,"Non-Specular Radar Cross Section Study," Technical Report AFAL- TR-73-422, Jan. 1974.

[4] R. F. Harrington and J. R. Mautz,"An Impedance Sheet Approximation for Thin Dielectric Shells," IEEE Trans. on Antennas and Propagat., Vol. AP-23, no. 4, July 1975.

[5] T. J. Peters, "Analysis of Matrix Elements Used in Program REST-E-STACK For Small Strip Separations ," Internal Memo no. 389055-003-M, March 28 1986.

Appendix E - Solution of the I. E. for Resistive Sheets H-Pol

I. Formulation of Integral Equation

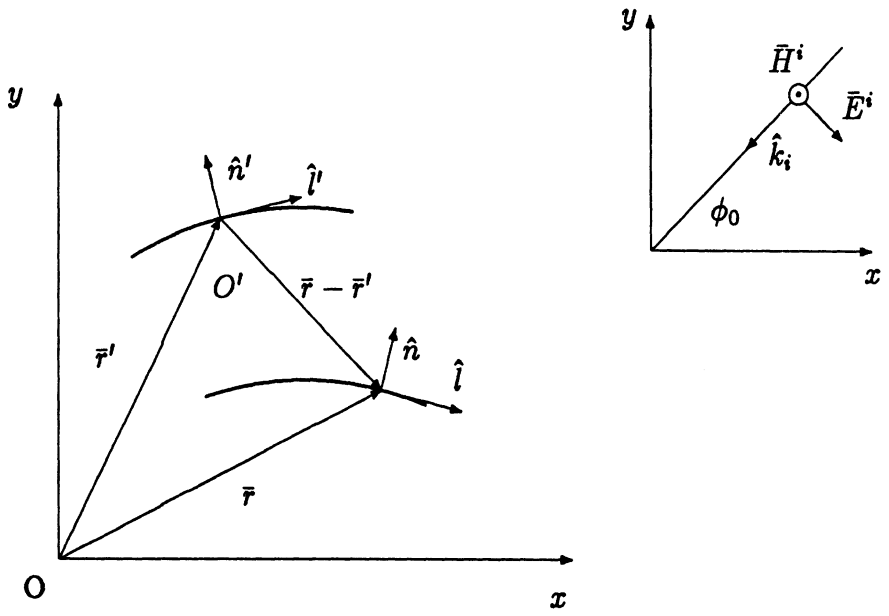

Fig. 1. General multiple strip configuration

The integral equation is formulated by equating the total field to the sum of the incident and scattered fields on the surface of each strip. Assume the $-i\omega t$ time convention is used such that the incident electric and magnetic fields may be described as

$$\bar{H}^i(\bar{r}) = H_{oi}e^{i(\bar{k}_i\cdot\bar{r})}\hat{z} = H_{oi}e^{-ik(x\cos(\phi_o)+y\sin(\phi_o))}\hat{z} \tag{1}$$

and

$$\bar{E}^i(\bar{r}) = -Z_o\hat{k}_i\times\bar{H}^i(\bar{r}) \tag{2}$$

where $k = \omega\sqrt{\mu_0\epsilon_0}$ is the freespace wave number, $Z_0 = \sqrt{\frac{\mu_0}{\epsilon_0}}$ is the characteristic wave impedance of free space and ϕ_0 is the angle of incidence. The induced electric current has only a tangential component and is assumed to vary only along the width of each strip.

$$\bar{K} = K_{l'}(x', y')\hat{l}' \tag{3}$$

From [1] define a Hertz vector of the electric kind as

$$\bar{\Pi}(\bar{R}) = \frac{iZ_o}{4\pi k}\int_{l'}\int_{-\infty}^{\infty}\hat{l}'K_{l'}(x', y')\frac{e^{ik\sqrt{(x-x')^2+(y-y')^2+(z-z')^2}}}{\sqrt{(x-x')^2+(y-y')^2+(z-z')^2}}dz'dl' \tag{4}$$

where

$$\bar{E}(\bar{R}) = \nabla\times\nabla\times\bar{\Pi}(\bar{R}) \tag{5}$$

$$\bar{H}(\bar{R}) = -i\frac{k}{Z_0}\nabla\times\bar{\Pi}(\bar{R}) \tag{6}$$

and $\bar{\Pi}$ satisfies the differential equation

$$\nabla^2\bar{\Pi}(\bar{R}) + k^2\bar{\Pi}(\bar{R}) = -\frac{i}{\omega\epsilon_0}\bar{J}(\bar{R}'). \tag{7}$$

The following integral identity reduces the formulation to two dimensions.

$$\int_{-\infty}^{\infty} \frac{e^{ik\sqrt{(x-x')^2+(y-y')^2+(z-z')^2}}}{\sqrt{(x-x')^2+(y-y')^2+(z-z')^2}} dz' = i\pi H_0^{(1)}\left(k\sqrt{(x-x')^2+(y-y')^2}\right) \tag{8}$$

The two dimensional Hertz vector is expressed as

$$\bar{\Pi}(x,y) = \frac{-Z_0}{4k}\int_{l'} \hat{l}' K_{l'}(x',y') H_0^{(1)}\left(k\sqrt{(x-x')^2+(y-y')^2}\right) dl'. \tag{9}$$

For convenience move the origin O to O' and make the substitution $\bar{\rho} = \bar{r} - \bar{r}'$ such that

$$\rho = |\bar{r} - \bar{r}'| \tag{10}$$

and

$$\hat{\rho} = \frac{\bar{r} - \bar{r}'}{|\bar{r} - \bar{r}'|}. \tag{11}$$

Thus (5) becomes

$$\bar{E}(\bar{r}) = \frac{-Z_0}{4k}\nabla \times \nabla \times \int_{l'} \hat{l}' K_{l'}(\bar{r}') H_0^{(1)}(k\rho) dl'. \tag{12}$$

The l' contour may be projected onto the $\rho - \phi$ plane and written in terms of un-primed unit vectors as

$$\hat{l}' = (\hat{l}' \cdot \hat{\rho})\hat{\rho} + (\hat{l}' \cdot \hat{\phi})\hat{\phi}. \tag{13}$$

The double curl operation may then be expanded as a normal and tangential derivative giving

$$\begin{aligned} \nabla \times \nabla \times H_0^{(1)}(k\rho)\hat{l}' &= \nabla \times \nabla \times \left[H_0^{(1)}(k\rho)(\hat{l}' \cdot \hat{\rho})\hat{\rho} + H_0^{(1)}(k\rho)(\hat{l}' \cdot \hat{\phi})\hat{\phi}\right] \\ &= \nabla \times \frac{1}{\rho}\left[\frac{\partial}{\partial \rho}(\rho H_0^{(1)}(k\rho)(\hat{l}' \cdot \hat{\phi})) - H_0^{(1)}(k\rho)\frac{\partial}{\partial \phi}(\hat{l}' \cdot \hat{\rho})\right]\hat{z} \end{aligned}$$

$$
\begin{aligned}
&= \nabla \times \frac{1}{\rho}\left[\frac{\partial}{\partial \rho}(\rho H_0^{(1)}(k\rho)) - H_0^{(1)}(k\rho)\right](\hat{l}' \cdot \hat{\phi})\hat{z} \\
&= -\nabla \times \left[(\hat{n}' \cdot \hat{\rho})\frac{\partial}{\partial \rho}H_0^{(1)}(k\rho)\right]\hat{z} \\
&= k\nabla \times \left[(\hat{n}' \cdot \hat{\rho})H_1^{(1)}(k\rho)\right]\hat{z} \\
&= k\nabla \left[(\hat{n}' \cdot \hat{\rho})H_1^{(1)}(k\rho)\right] \times \hat{l} \times \hat{n} \\
&= k\left(\hat{n} \cdot \nabla \left[(\hat{n}' \cdot \hat{\rho})H_1^{(1)}(k\rho)\right]\right)\hat{l} - k\left(\hat{l} \cdot \nabla \left[(\hat{n}' \cdot \hat{\rho})H_1^{(1)}(k\rho)\right]\right)\hat{n} \\
&= k\left[\frac{\partial}{\partial n}\hat{l} - \frac{\partial}{\partial l}\hat{n}\right]\left[(\hat{n}' \cdot \hat{\rho})H_1^{(1)}(k\rho)\right]. \qquad (14)
\end{aligned}
$$

Thus, the scattered electric field will then be of the form

$$
\bar{E}^s(\bar{r}) = -\frac{Z_0}{4}\left[\frac{\partial}{\partial n}\hat{l} - \frac{\partial}{\partial l}\hat{n}\right]\int_{l'}\left[(\hat{n}' \cdot \hat{\rho})K_{l'}(x', y')H_1^{(1)}(k\rho)\right]dl' \qquad (15)
$$

and the total tangential electric field on the surface of each strip is equal to the sum of the incident plus the scattered tangential components.

$$
E_l^t(x, y) = E_l^i(x, y) - \frac{Z_0}{4}\frac{\partial}{\partial n}\int_{l'}\left[(\hat{n}' \cdot \hat{\rho})K_{l'}(x', y')H_1^{(1)}(k\rho)\right]dl' \qquad (16)
$$

In order to solve the equation, the boundary condition on the surface of each strip must be postulated.

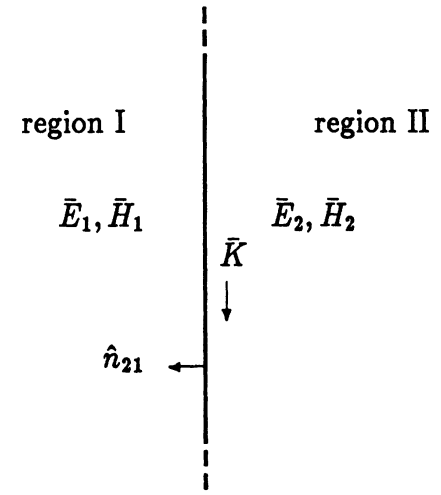

Fig. 2. Boundary of resistive strip

$$\hat{n}_{21} \times (\bar{E}_1 - \bar{E}_2) = 0 \tag{17}$$

$$\hat{n}_{21} \times (\bar{H}_1 - \bar{H}_2) = \bar{K} = \frac{\bar{E}_1 - (\hat{n}_{21} \cdot \bar{E}_1)\hat{n}_{21}}{R} = \frac{\bar{E}_2 - (\hat{n}_{21} \cdot \bar{E}_2)\hat{n}_{21}}{R} \tag{18}$$

$$\hat{n}_{21} \times (\bar{D}_1 - \bar{D}_2) = \rho_s = \frac{1}{i\omega} \nabla \cdot \bar{K} \tag{19}$$

$$\hat{n}_{21} \times (\bar{B}_1 - \bar{B}_2) = 0 \tag{20}$$

Observation of (18) shows that the total tangential electric field may be related to the surface resistance and the surface current. For convenience, define the resistance normalized to the freespace impedance as η.

$$E_l^t = Z_0 \eta K_l. \tag{21}$$

Substituting (21) into (16) yields an integral equation enforced on the surface of each strip given as

$$4\eta(x,y)K_l(x,y) + \frac{\partial}{\partial n} \int_{l'} \left[(\hat{n}' \cdot \hat{\rho}) K_{l'}(x',y') H_1^{(1)}(k\rho) \right] dl' = \frac{4}{Z_0} E_l^i(x,y). \tag{22}$$

II. Solution Using Method of Weighted Residuals

On the surface of the strip define the residual as the sum of the tangential incident and scattered fields minus the total field such that $Residual = E_l^i(l) + E_l^s(l) - E_l^t(l)$. The method of weighted residuals is used to set the integral of a weighting function $w(l)$ times the residual equal to zero. This satisfies the boundary condition in an average sense as opposed to at discrete points. Let each strip be composed of cells with arc length δ and assume the current is approximated by a series of expansion functions with constant coefficients.

$$K(l') = \sum_{q=1}^{N} K(q)L(l') \tag{23}$$

$$L(l') = \begin{cases} h(l') & l_q - \frac{\delta_q}{2} \leq l' \leq l_q + \frac{\delta_q}{2} \\ 0 & \text{otherwise} \end{cases} \tag{24}$$

Equation (22) may be solved discretely by substituting in (23) and integrating both sides with respect to a weight function. Let p denote the integration of the residual times the weighting function over the pth observation cell element. Let q denote the integration of the expansion function times the kernel over the qth source cell element. The system of equations may be written in a compact form as

$$\sum_{p=1}^{N} \left[u(p)K(p) + \sum_{q=1}^{N} f(p,q)K(q) = v(p) \right] \tag{25}$$

where

$$u(p) = 4 \int_{l_p - \frac{\delta_p}{2}}^{l_p + \frac{\delta_p}{2}} w(l)\eta(l)h(l)dl \tag{26}$$

$$v(p) = \frac{4}{Z_0} \int_{l_p - \frac{\delta_p}{2}}^{l_p + \frac{\delta_p}{2}} w(l)E_l^i(l)dl \tag{27}$$

$$f(p,q) = \int_{l_p-\frac{\delta_p}{2}}^{l_p+\frac{\delta_p}{2}} w(l) \left[\int_{l_q-\frac{\delta_q}{2}}^{l_q+\frac{\delta_q}{2}} h(l')g(l,l')dl' \right] dl \tag{28}$$

and

$$\begin{aligned} g(l,l') &= \frac{\partial}{\partial n}\left[(\hat{n}'\cdot\hat{\rho})H_1^{(1)}(k\rho)\right] \\ &= \hat{n}\cdot\left[(\hat{n}'\cdot\hat{\rho})\frac{\partial}{\partial\rho}H_1^{(1)}(k\rho)\hat{\rho} + \frac{1}{\rho}H_1^{(1)}(k\rho)(\hat{n}'\cdot\frac{\partial\hat{\rho}}{\partial\phi})\hat{\phi}\right] \\ &= k(\hat{n}'\cdot\hat{\rho})(\hat{n}\cdot\hat{\rho})H_1^{(1)'}(k\rho) + \frac{1}{\rho}(\hat{n}'\cdot\hat{\phi})(\hat{n}\cdot\hat{\phi})H_1^{(1)}(k\rho) \\ &= k(\hat{n}'\cdot\hat{\rho})(\hat{n}\cdot\hat{\rho})H_1^{(1)'}(k\rho) + \frac{1}{\rho}(\hat{l}'\cdot\hat{\rho})(\hat{l}\cdot\hat{\rho})H_1^{(1)}(k\rho) \\ &= \frac{1}{\rho}\left[(\hat{l}'\cdot\hat{\rho})(\hat{l}\cdot\hat{\rho}) - (\hat{n}'\cdot\hat{\rho})(\hat{n}\cdot\hat{\rho})\right]H_1^{(1)}(k\rho) + k(\hat{n}'\cdot\hat{\rho})(\hat{n}\cdot\hat{\rho})H_0^{(1)}(k\rho). \end{aligned} \tag{29}$$

III. Application to Parallel Stacked Resistive Strips

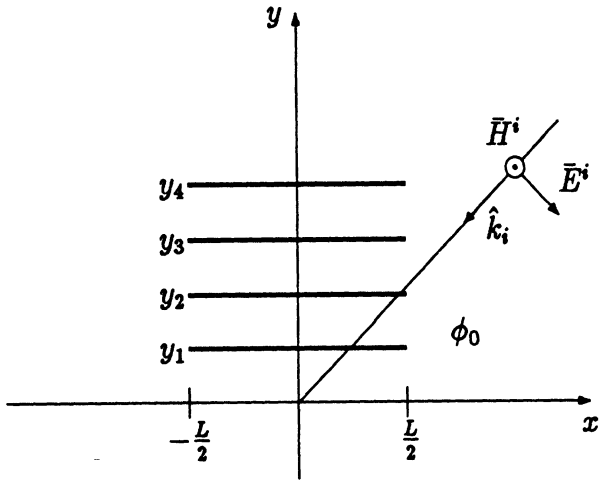

Fig. 3. Geometry of stacked resistive strips

The simplest representative case of multiple resistive strips is shown in Fig. 3. Let δ be the cell width and N the total number of cells.

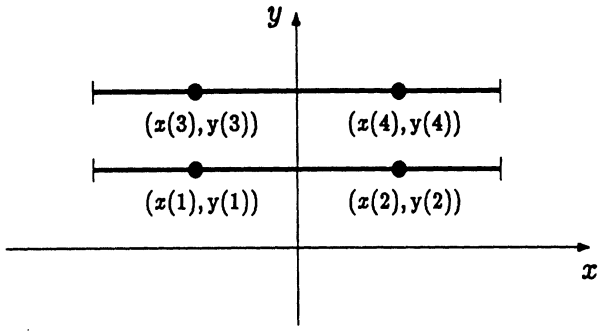

Fig. 4. Two strips with a total of 4 cells

The matrix form of (25) for the geometry shown in Fig. 4 is written as

$$\begin{bmatrix} u_1+f_{11} & f_{12} & f_{13} & f_{14} \\ f_{21} & u_2+f_{22} & f_{23} & f_{24} \\ f_{31} & f_{32} & u_3+f_{33} & f_{34} \\ f_{41} & f_{42} & f_{43} & u_4+f_{44} \end{bmatrix} \begin{bmatrix} K_1 \\ K_2 \\ K_3 \\ K_4 \end{bmatrix} = \begin{bmatrix} v_1 \\ v_2 \\ v_3 \\ v_4 \end{bmatrix} \tag{30}$$

Observation of (30) shows that the surface resistance and the self cell contributions are the diagonal elements of the matrix.

Assume that the expansion function is a pulse and the weighting function is a delta function.

$$h(l') = h(x',y') = \begin{cases} 1 & x_q - \frac{\delta}{2} \le x' \le x_q + \frac{\delta}{2} \quad y' = \text{constant} \\ 0 & \text{otherwise} \end{cases} \tag{31}$$

$$w(l) = w(x,y) = \begin{cases} \delta(x-x_p) & x_p - \frac{\delta}{2} \le x \le x_p + \frac{\delta}{2} \quad y = \text{constant} \\ 0 & \text{otherwise} \end{cases} \tag{32}$$

For the geometry of Fig. 3. $\hat{l} = \hat{x}$ and $\hat{n} = \hat{y}$.

$$g(l,l') = g(x,y,x',y') = ((x-x')^2 - (y-y')^2)\frac{H_1^{(1)}(k\rho)}{\rho^3} + k(y-y')^2\frac{H_0^{(1)}(k\rho)}{\rho^2} \tag{33}$$

$$f(p,q) = \int_{x_q-\frac{\delta}{2}}^{x_q+\frac{\delta}{2}} g(x_p, y_p, x', y_q)dx' \tag{34}$$

Case I - non-singular integrand

If cell(p)≠cell(q) and $|y_p - y_q| \geq \delta$ then the observation point is greater than or equal to one cell length away from the source point. Simpson's three point composite rule is used to numerically solve for $f(p,q)$. Each cell interval δ is broken up into $2M$ subintervals.

$$\int_a^b f(x)dx = \frac{h}{3}\left[f(a) + 2\sum_{n=1}^{M-1} f(x_{2n}) + 4\sum_{n=1}^{M} f(x_{2n-1}) + f(b)\right] \tag{35}$$

where

$$h = \frac{b-a}{2M} \tag{36}$$

$$x_{2n} = a + 2nh \tag{37}$$

and

$$x_{2n-1} = a + (2n-1)h. \tag{38}$$

Thus

$$\begin{aligned} f(p,q) &= \frac{h}{3}\left[g\left(x_p, y_p, x_q - \frac{\delta}{2}, y_q\right) + g\left(x_p, y_p, x_q + \frac{\delta}{2}, y_q\right)\right] \\ &\quad +2\frac{h}{3}\left[\sum_{n=1}^{M-1} g(x_p, y_p, x_{q2n}, y_q) + 2\sum_{n=1}^{M} g(x_p, y_p, x_{q(2n-1)}, y_q)\right] \end{aligned} \tag{39}$$

where

$$h = \frac{\delta}{2M} \tag{40}$$

$$x_{q2n} = x_q - \frac{\delta}{2} + 2nh \tag{41}$$

and

$$x_{q(2n-1)} = x_q - \frac{\delta}{2} + (2n-1)h. \tag{42}$$

Case II - singular integrand

If cell(p)=cell(q) or $|y_p - y_q| \leq \delta$ then the observation point is less than or equal to one cell length away from the source point and the integrand becomes unbounded. It is more conveinent to use an equivalent form of $g(l, l')$.

$$g(l, l') = -\frac{1}{k}\frac{\partial^2}{\partial y^2} H_0^{(1)}(k\rho) \tag{43}$$

The small argument approximation of the Hankel function is then integrated analytically. From [2]

$$H_0^{(1)}(z) = J_0(z) + iN_0(z) \tag{44}$$

where

$$J_0(z) = \sum_{m=0}^{\infty} \frac{(-1)^m}{(m!)^2} \left(\frac{z}{2}\right)^{2m} \tag{45}$$

and

$$N_0(z) = \frac{2}{\pi}\left(ln\left(\frac{z}{2}\right) + \gamma\right) J_0(z) - \frac{2}{\pi} \sum_{m=1}^{\infty} \frac{(-1)^m}{(m!)^2} \left(\frac{z}{2}\right)^{2m} \sum_{s=1}^{m} \left(\frac{1}{s}\right). \tag{46}$$

Combining (45) and (46) for $m = 1$

$$H_0^{(1)}(z) = c_1 - c_2 z^2 + i\frac{2}{\pi} ln(z) - i\frac{1}{2\pi} z^2 ln(z) + O(z^4) \tag{47}$$

where

$$c_1 = 1 + i\frac{2}{\pi}(\gamma - ln(2)) \tag{48}$$

$$c_2 = \frac{1}{4} + i\frac{1}{2\pi}(\gamma - 1 - ln(2)) \tag{49}$$

and $\gamma = 0.5772157$ is known as Euler's constant. Let $d = y - y' = y_p - y_q$. Then

$$f(p, q) = -\frac{1}{k}(I_1 + I_2 + I_3) \tag{50}$$

where

$$I_1 = i\frac{2}{\pi}\frac{\partial^2}{\partial d^2}\int_{x_q-\frac{\delta}{2}}^{x_q+\frac{\delta}{2}} ln\left(k\sqrt{(x_p-x')^2+d^2}\right)dx' \tag{51}$$

$$I_2 = -k^2c_2\frac{\partial^2}{\partial d^2}\int_{x_q-\frac{\delta}{2}}^{x_q+\frac{\delta}{2}} \left((x_p-x')^2+d^2\right)dx' \tag{52}$$

and

$$I_3 = -i\frac{k^2}{2\pi}\frac{\partial^2}{\partial d^2}\int_{x_q-\frac{\delta}{2}}^{x_q+\frac{\delta}{2}} \left((x_p-x')^2+d^2\right) ln\left(k\sqrt{(x_p-x')^2+d^2}\right)dx'. \tag{53}$$

Making the substitution $t = x_p - x'$, the three integrals may be written as

$$I_1 = i\frac{2}{\pi}\frac{\partial^2}{\partial d^2}\int_{x_p-x_q-\frac{\delta}{2}}^{x_p-x_q+\frac{\delta}{2}} ln\left(k\sqrt{t^2+d^2}\right)dt \tag{54}$$

$$I_2 = -k^2c_2\frac{\partial^2}{\partial d^2}\int_{x_p-x_q-\frac{\delta}{2}}^{x_p-x_q+\frac{\delta}{2}} \left(t^2+d^2\right)dt \tag{55}$$

and

$$I_3 = -i\frac{k^2}{2\pi}\frac{\partial^2}{\partial d^2}\int_{x_p-x_q-\frac{\delta}{2}}^{x_p-x_q+\frac{\delta}{2}} \left(t^2+d^2\right) ln\left(k\sqrt{t^2+d^2}\right)dt. \tag{56}$$

In general these integrals are not symmetric in t. However, for the special case where the observation cell and the source cell have the same horizontal position such that $x_p = x_q$, the limits are symmetric and the algebra is much easier. The integrals are simplified as

$$I_1 = i\frac{4}{\pi}\frac{\partial^2}{\partial d^2}\int_0^{\frac{\delta}{2}} ln\left(k\sqrt{t^2+d^2}\right)dt \tag{57}$$

$$I_2 = -2k^2c_2\frac{\partial^2}{\partial d^2}\int_0^{\frac{\delta}{2}} \left(t^2+d^2\right)dt \tag{58}$$

and

$$I_3 = -i\frac{k^2}{\pi}\frac{\partial^2}{\partial d^2}\int_0^{\frac{\delta}{2}} \left(t^2+d^2\right) ln\left(k\sqrt{t^2+d^2}\right)dt. \tag{59}$$

Using the integral identity

$$\int ln(a^2+x^2)dx = xln(a^2+x^2) - 2x + 2atan^{-1}\left(\frac{x}{a}\right) \tag{60}$$

I_1 is evaluated as

$$I_1 = i\frac{4}{\pi}\frac{\partial^2}{\partial d^2}\left[\frac{\delta}{2}ln\left(\frac{k}{2}\sqrt{\delta^2+4d^2}\right) - \frac{\delta}{2} + dtan^{-1}\left(\frac{\delta}{2d}\right)\right] \tag{61}$$

and after the differentiation is completed

$$I_1 = -i\frac{8}{\pi}\left[\frac{\delta}{\delta^2+4d^2}\right]. \tag{62}$$

I_2 may be written down by inspection as

$$I_2 = -2k^2\delta c_2. \tag{63}$$

Using the integral identity

$$\int (a^2+x^2)ln(a^2+x^2)dx = x\left(\frac{x^2}{3}+a^2\right)ln(a^2+x^2) + \frac{4}{3}a^3tan^{-1}\left(\frac{x}{a}\right) - \frac{4}{3}a^2x - \frac{2}{9}x^3 \tag{64}$$

I_3 is evaluated as

$$I_3 = -i\frac{k^2}{\pi}\frac{\partial^2}{\partial d^2}\left[\frac{\delta}{2}\left(\frac{\delta^2}{12}+d^2\right)ln\left(\frac{k}{2}\sqrt{4d^2+\delta^2}\right) + \frac{2}{3}d^3tan^{-1}\left(\frac{\delta}{2d}\right) - \frac{1}{3}\delta d^2 - \frac{\delta^3}{72}\right] \tag{65}$$

and after the differentiation is completed

$$I_3 = -i\frac{k^2}{\pi}\delta\left[ln\left(\frac{k}{2}\sqrt{\delta^2+4d^2}\right) + 4\frac{d}{\delta}tan^{-1}\left(\frac{\delta}{2d}\right) - \frac{1}{2}\right]. \tag{66}$$

For $d = 0$ the self cell value is given as

$$f(p,q) = k\delta\left[\frac{1}{2} + i\frac{1}{\pi}\left(\gamma - \frac{3}{2} + \frac{8}{(k\delta)^2} + ln\left(\frac{k\delta}{4}\right)\right)\right]. \tag{67}$$

Elements affected by case II occur along the diagonals of the matrix. This may be observed by viewing the matrix derived from the geometry shown in Fig. 5.

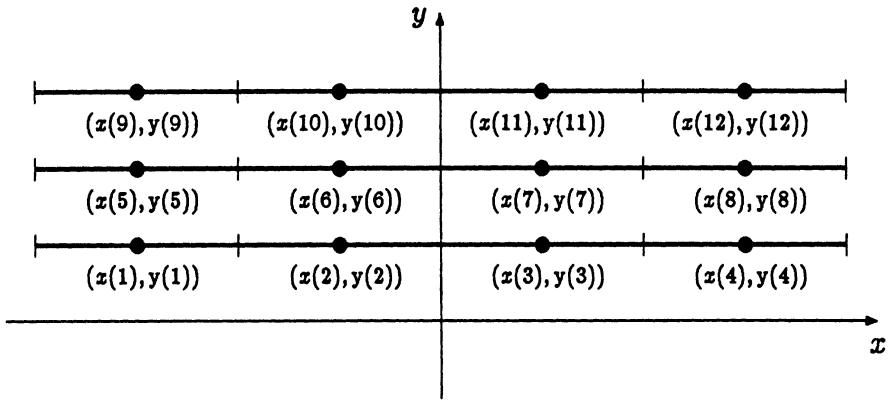

Fig. 5. Three strips with a total of 12 cells

The system of equations for Fig. 5 is written in matrix form as

$$[S][K] = [V]. \tag{68}$$

If the cell width and resistance are the same and constant for each strip then $[S]$ is a block Toeplitz matrix. This means that $[S]$ and all sub matrices $[S]_{mn}$ are Toeplitz. A Toeplitz matrix is one that is symmetric and all the elements on a particular diagonal are the same.

$$[S] = \begin{bmatrix} [S]_{11} & [S]_{12} & [S]_{13} \\ [S]_{12} & [S]_{11} & [S]_{12} \\ [S]_{13} & [S]_{12} & [S]_{11} \end{bmatrix} \tag{69}$$

The case II terms make up the diagonals of all $[S]_{mn}$ for $m \neq n$ the self cell terms comprise the diagonal elements of $[S]_{mm}$. The distinction between case I and case II becomes critical as $|y_p - y_q| \rightarrow 0$ for $x_p = x_q$. If $|y_p - y_q| = d$ then the

graph of $|f(p,q)|$ as a function of $\frac{d}{\delta}$ for $0 \leq \frac{d}{\delta} \leq 1$ is given by Fig. 6.

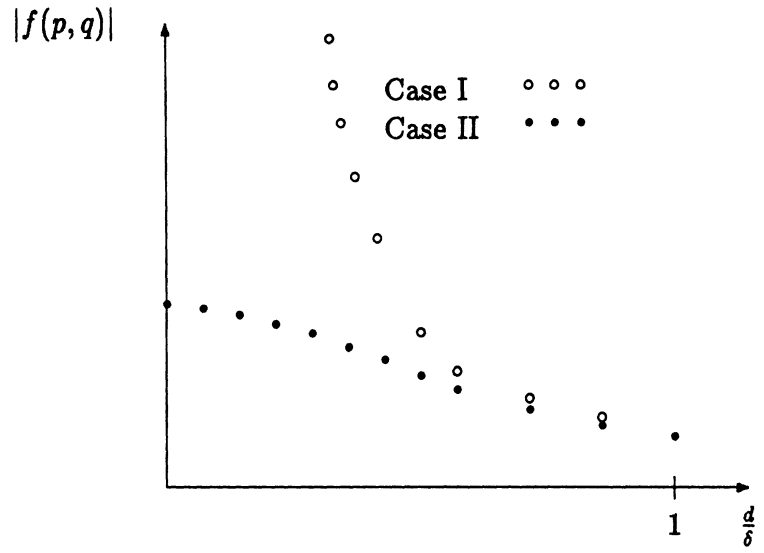

Fig. 6. Matrix elements vs vertical spacing

Fig. 6 shows that case II elements remain finite and approach the self cell value as the spacing between two strips approaches zero compared with case I elements which increase without bound. A more detailed analysis of the data shown in Fig. 6 is given in [5].

IV. Calculation of Scattered Magnetic Field

The scattered magnetic field given in (6) may be calculated using (9) and (14).

$$\begin{aligned} \bar{H}^s(\bar{r}) &= \frac{i}{4}\nabla \times \int_{l'} \hat{l}' K_{l'}(\bar{r}') H_0^{(1)}(k\rho) dl' \\ &= i\frac{k}{4}\hat{z} \int_{l'} (\hat{n}' \cdot \hat{\rho}) K_{l'}(\bar{r}') H_1^{(1)}(k\rho) dl' \end{aligned} \tag{70}$$

In the far zone

$$H_1^{(1)}(k\rho) \approx -i\sqrt{\frac{2}{\pi k\rho}}e^{-i\frac{\pi}{4}}e^{ik\rho} \tag{71}$$

where

$$\rho = \begin{cases} r - \hat{r}\cdot\bar{r}' & \text{numerator} \\ r & \text{denominator} \end{cases} \tag{72}$$

such that

$$H_1^{(1)}(k\,|\bar{r}-\bar{r}'|) \approx -i\sqrt{\frac{2}{\pi kr}}e^{-i\frac{\pi}{4}}e^{ikr}e^{-ik(x'cos(\phi)+y'sin(\phi))}. \tag{73}$$

Substituting (73) into (70)

$$\begin{aligned} \bar{H}^s(\bar{r}) &= \hat{z}\sqrt{\frac{k}{8\pi r}}e^{-i\frac{\pi}{4}}e^{ikr}\int_{l'}(\hat{n}'\cdot\hat{r})K_{l'}(x',y')e^{-ik(x'cos(\phi)+y'sin(\phi))}dl' \\ &= \hat{z}\sqrt{\frac{k}{8\pi r}}e^{-i\frac{\pi}{4}}e^{ikr}sin(\phi)\sum_{q=1}^{N}K_x(q)e^{-iky_qsin(\phi)}\int_{x_q-\frac{\delta}{2}}^{x_q+\frac{\delta}{2}}e^{-ikrcos(\phi)}d\tau \\ &= \hat{z}\sqrt{\frac{k}{8\pi r}}e^{-i\frac{\pi}{4}}e^{ikr}\delta sin(\phi)\sum_{q=1}^{N}K_x(q)e^{-ik(x_qcos(\phi)+y_qsin(\phi))}. \end{aligned} \tag{74}$$

V. Calculation of Radar Cross Section

The radar cross section σ is defined as

$$\begin{aligned} \sigma &= \lim_{r\to\infty}\left[2\pi r\frac{|\bar{H}^s|^2}{|\bar{H}^i|^2}\right] \\ &= \frac{k}{4}(\delta sin(\phi))^2\left|\sum_{q=1}^{N}K_x(q)e^{-ik(x_qcos(\phi)+y_qsin(\phi))}\right|^2. \end{aligned} \tag{75}$$

REFERENCES

[1] J. A. Stratton, Electromagnetic Theory. New York: McGraw-Hill, 1941, pp. 430-431.

[2] P. M. Morse and H. Feshbach, Methods of Theoretical Physics. New York: McGraw-Hill, 1953, Part I, p. 627.

[3] E. F. Knott and T. B. A. Senior,"Non-Specular Radar Cross Section Study," Technical Report AFAL- TR-73-422, Jan. 1974.

[4] R. F. Harrington and J. R. Mautz,"An Impedance Sheet Approximation for Thin Dielectric Shells," IEEE Trans. on Antennas and Propagat., Vol. AP-23, no. 4, July 1975.

[5] T. J. Peters, "Analysis of Matrix Elements Used in Program REST-H-STACK For Small Strip Separations ," Internal Memo no. 389055-008-M, March 28, 1986.